

# Rising Up: Hierarchical Metal–Organic Frameworks in Experiments and Simulations

Yi Luo, Momin Ahmad, Alexander Schug,\* and Manuel Tsotsalas\*

Controlled synthesis across several length scales, ranging from discrete molecular building blocks to size- and morphology-controlled nanoparticles to 2D sheets and thin films and finally to 3D architectures, is an advanced and highly active research field within both the metal–organic framework (MOF) domain and the overall material science community. Along with synthetic progress, theoretical simulations of MOF structures and properties have shown tremendous progress in both accuracy and system size. Further advancements in the field of hierarchically structured MOF materials will allow the optimization of their performance; however, this optimization requires a deep understanding of the different synthesis and processing techniques and an enhanced implementation of material modeling. Such modeling approaches will allow us to select and synthesize the highest-performing structures in a targeted rational manner. Here, recent progress in the synthesis of hierarchically structured MOFs and multiscale modeling and associated simulation techniques is presented, along with a brief overview of the challenges and future perspectives associated with a simulation-based approach toward the development of advanced hierarchically structured MOF materials.

and signal transduction. These molecular components are then organized into sub-cellular and cellular compartments or domains. These subcellular and cellular compartments are then structured into different organs and organ systems, which ultimately, at the highest level, constitute the entire organism. These organisms are then able to self-replicate and are themselves part of more complex ecosystems.

Hierarchically organized synthetic materials also contain structural elements at more than one length scale. This structural hierarchy can strongly influence bulk material properties. Understanding the effects of hierarchical structure is essential for guiding the synthesis of new materials with properties that are tailored to specific applications.<sup>[2]</sup> The individual building blocks in a material, which are often grouped into different sub-domains and domains, are usually regarded as structural elements in hierarchical materials. However, other features of materials,

such as porosity or chemical composition, can also be organized hierarchically, which is crucial for optimizing specific properties, such as diffusion within a material or directional energy transfer.<sup>[3]</sup> The hierarchical order of a material may be defined as the number ( $n$ ) of levels of scale within a specific structure.<sup>[2]</sup> As in natural systems, such as proteins, one can categorize structures at different length scales starting from the smallest length scale as primary structures, secondary structures, tertiary structures, and so on.<sup>[4]</sup>


Metal–organic frameworks (MOFs) are a class of functional crystalline materials that has received increasing attention over the

## 1. Introduction

Hierarchical organization is a basic principle found in many natural, technical, and social systems.<sup>[1]</sup> The human body, in fact, is a classic example of hierarchical organization. At the lowest level, simple molecular building blocks, such as amino acids or lipids, create 3D biomolecular machines able to perform complex tasks, including data storage as genes on DNA; the control, readout, and translation of genes into encoded proteins; catalytic functions; energy storage and consumption;

Y. Luo, Dr. M. Tsotsalas  
Institute of Functional Interfaces (IFG)  
Karlsruhe Institute of Technology (KIT)  
Hermann-von-Helmholtz-Platz 1, D-76344 Eggenstein-Leopoldshafen  
Germany  
E-mail: manuel.tsotsalas@kit.edu

M. Ahmad  
Steinbuch Centre for Computing  
Karlsruhe Institute of Technology (KIT)  
Hermann-von-Helmholtz-Platz 1, D-76344 Eggenstein-Leopoldshafen  
Germany

 The ORCID identification number(s) for the author(s) of this article can be found under <https://doi.org/10.1002/adma.201901744>.

© 2019 The Authors. Published by WILEY-VCH Verlag GmbH & Co. KGaA, Weinheim. This is an open access article under the terms of the Creative Commons Attribution-NonCommercial License, which permits use, distribution and reproduction in any medium, provided the original work is properly cited and is not used for commercial purposes.

DOI: 10.1002/adma.201901744

M. Ahmad  
Institute for Theoretical Solid State Theory  
Karlsruhe Institute of Technology (KIT)  
Wolfgang-Gaede-Str. 1, D-76131 Karlsruhe, Germany

Dr. A. Schug  
John von Neumann Institute for Computing  
Jülich Supercomputer Centre  
Forschungszentrum Jülich  
Wilhelm-Johnen-Straße, 52428 Jülich, Germany  
E-mail: al.schug@fz-juelich.de

Dr. M. Tsotsalas  
Institute of Organic Chemistry (IOC)  
Karlsruhe Institute of Technology (KIT)  
Fritz-Haber-Weg 6, D-76131 Karlsruhe, Germany

last 20 years.<sup>[5]</sup> MOFs have two components: metal ion or metal oxo clusters, which act as nodes, and organic molecules, which act as linkers between the nodes. Due to the wide variety of suitable organic molecules and metal nodes, more than 70 000 different MOF crystal structures have already been reported.<sup>[6]</sup>

The large variability of MOFs in terms of their: i) framework architectures, ii) pore structures, and iii) functional constituents permits MOF materials to be hierarchically structured using three approaches: according to architecture, according to porosity, or according to the composition. The basic structures and compositions of MOF materials and the different approaches to their hierarchical structuring are shown in **Figure 1**.

MOF materials with hierarchical architectures have defined structures on multiple length scales. All MOFs have defined framework structures on the molecular level (in the range of several angstroms to several nm), which is largely defined by the choice of the molecular components. This molecular-level framework represents the primary structure. To create secondary or higher-order structures, one needs to additionally control MOF materials at a larger length scale, from several tens of nm to  $\mu\text{m}$  to mm, up to the macroscopic level.

Most MOF types are intrinsically porous because the defined framework structure contains potential voids at the microporous (pore sizes less than 2 nm) to mesoporous (pore sizes between 2 and 50 nm) length scales. These potential voids represent the primary porosity.<sup>[7]</sup> Introducing a secondary porosity at a larger length scale creates hierarchically porous materials. Here, one must keep in mind that the porosity of a specific MOF is closely linked to its framework structure.

The diversity of organic linkers and metal nodes suitable for synthesizing MOFs makes it possible to prepare numerous compounds, even for a single defined framework topology.<sup>[8]</sup> Since the organization of molecular components is defined at the molecular scale, one can hierarchically organize MOF materials by inserting different components at a larger length scale.<sup>[9,10]</sup> **Table 1** summarizes the different types of hierarchies in MOFs, along with their



**Alexander Schug** received his Diploma and Ph.D. in physics from the University of Dortmund (Germany). He was a postdoctoral fellow at the Kobe University (Japan) and University of California, San Diego (USA) before he became assistant professor at the University of Umeå (Sweden). He then headed a research group at Karlsruhe

Institute of Technology (Germany) and is currently additionally heading a Neumann Institute of Computing Group at Research Centre Jülich (Germany).



**Manuel Tsotsalis** studied chemistry at the University of Münster, where he received his Diploma in 2006 and his Ph.D. in 2010. After a postdoctoral stay at Kyoto University, he joined the Karlsruhe Institute of Technology (KIT) in 2013, where he is currently leading a Helmholtz young investigator group, hosted at

the Institute of Functional Interfaces and the Institute of Organic Chemistry. His research interests focus on the interfacial synthesis and hierarchical structuring of metal-organic frameworks (MOF) and porous polymers for application as nanomembranes and bioactive surface coatings.

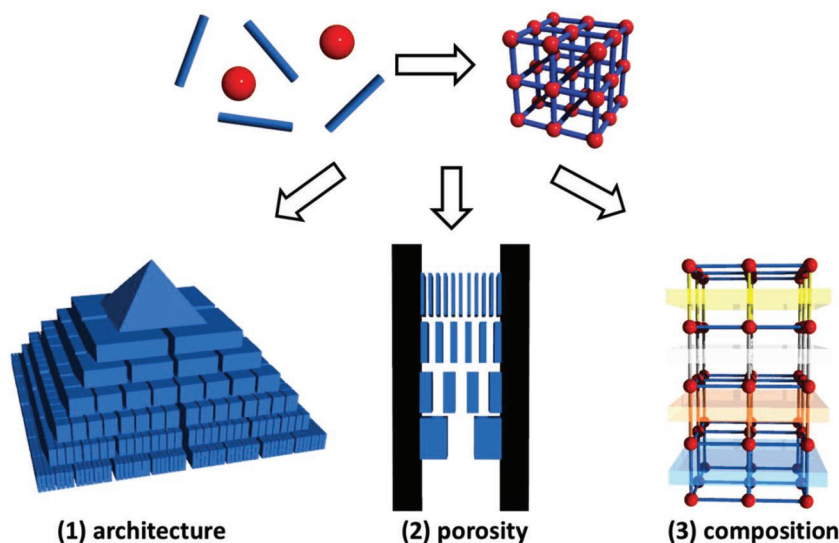


**Figure 1.** Top: Metal-organic frameworks prepared by self-assembly of metal nodes and organic linkers. Bottom: Different perspectives of hierarchical structuring in metal-organic frameworks 1) hierarchical architecture, 2) hierarchical porosity, and 3) hierarchical composition.

characteristics and properties, and offers some related examples from natural systems.

The hierarchy type of a MOF greatly influences the final properties of the bulk material, and the three hierarchy types can provide complementary qualities. As evidenced in many biological materials, such as horn, wood, or bone, hierarchical architectures provide materials with exceptional mechanical strengths and unique material properties.<sup>[11]</sup> Hierarchical porosity, in contrast, enables fast transport and/or a high degree of flow distribution within a bulk material.<sup>[12]</sup> Compositional hierarchy can provide a protective layer or, if desired, promote the directional transport of ions or energy (e.g., in membranes or light-harvesting materials in solar cells).<sup>[13]</sup>

The experimental insight gained by developing more complex MOF-based materials has generated a high demand for in-silico modeling of these materials. This demand stems both from a desire to understand the basic principles leading to specific material

**Table 1.** Different types of hierarchies in MOFs, their characteristics, properties, and related examples in natural systems.

Type of hierarchy	Characteristics	Properties	Examples in natural systems
Architecture	Structural elements on more than one length scale	Optimized mechanical strength and rupture resistance	Tree
Porosity	Porosity on more than one length scale	Optimized mass flow combined with high surface area and accessibility	Lung
Composition	Organization of functional units on more than one length scale	Protective coatings/layers or optimized energy transfer	Skin

properties and from the promise of accelerated development cycles by complementing the experimental insights. Multiple disciplines such as material science, physics, chemistry, and the life sciences have a long tradition of honing their specific simulation techniques to better understand and design their individual systems of interest. The ongoing exponential growth of computational power and data storage capabilities accelerates the possible insight from such simulations, often by complementary experimental and simulation studies.<sup>[14]</sup>

In the following sections, we will provide an overview and analysis of the current status of hierarchically structured MOF material synthesis and the multiscale modeling and associated simulation techniques employed in designing these molecular materials. We will complement the discussion of the basic challenges and fundamental aspects in the synthesis of MOF materials associated with the introduction of hierarchical architectures, porosities, and compositions with guidelines for simulations across different length scales, which will help to implement a simulation-based approach toward the design of hierarchically structured MOF materials with optimized properties.

### 1.1. Introduction to the Synthesis of Hierarchical MOF Materials

Introducing hierarchy into a MOF material can be realized either by controlling the conditions during MOF growth or by postsynthetic treatment of a material. In this regard, hierarchical MOF materials can be categorized into bottom-up and top-down approaches.

MOFs are synthesized via self-assembly/crystallization of metal nodes (ions or clusters) connected by organic molecular linkers. This synthesis is characterized by two processes: nucleation and growth. To create higher-order MOF structures, one has to control both nucleation and growth processes with high spatial and temporal resolution.<sup>[15]</sup> Nucleation is highly dependent on the concentration of the reactants in the solution, and the relationship can be described by the LaMer burst nucleation diagram shown in **Figure 2**.<sup>[16]</sup>

Usually, MOF precursors form a stable solution at low concentrations. Once the concentration is increased above the saturation threshold ( $C_{\min}$ ), nucleation can occur at a certain rate depending on the solvent and temperature used in the synthesis. If the concentration reaches a critical limiting supersaturation threshold ( $C_{\max}$ ), nucleation occurs instantaneously from solution.

As a general guideline, to create hierarchical MOF structures in a bottom-up approach, one needs to achieve a high supersaturation of metal centers and organic linkers within a

locally confined area. To create hierarchical MOF structures in a top-down approach, one needs to synthesize MOFs with low nucleation rates, which allows the growth of a few larger crystals that can be substructured using different postsynthetic treatment strategies. The different strategies for bottom-up and top-down syntheses of hierarchical MOF structures will be discussed in detail in the corresponding sections below.

### 1.2. Introduction to the Simulation of Hierarchical MOF Materials

Advanced simulation techniques can complement experiments in a variety of fields, ranging from simulating biologically relevant molecules such as proteins or RNA<sup>[14d,17,18]</sup> with atomic resolution for applications in molecular electronics<sup>[19]</sup> to descriptions of material properties.<sup>[20]</sup> All these applications strike a good balance between the desired level of detail and the computational expense. The involved methods can be broadly divided into methods based on computationally demanding quantum mechanics (QM), in particular on density functional theory (DFT),<sup>[21]</sup> and those based on the less computationally demanding molecular mechanics (MM).<sup>[18]</sup>

The computational complexity of DFT calculations comes from calculating the full electron density of each molecule to predict the physical properties of a material. DFT calculations,

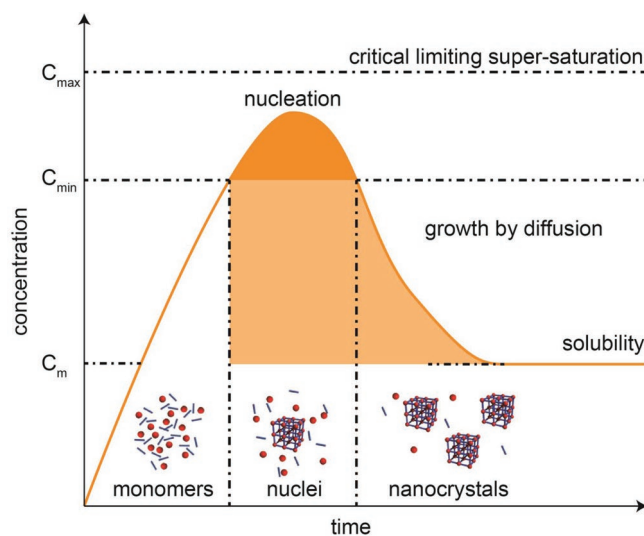


**Figure 2.** LaMer burst nucleation diagram showing the relationship between nucleation and concentration of reactants in solution.<sup>[16]</sup>

which are expensive and very time-consuming, are not suitable to calculate crystal structures with many hundreds of thousands of atoms. By contrast, MM is based on simple interactions, such as springs between point-like atoms. Here, force fields contain parameters to calculate energetic contributions for the atomic interactions in a given structure or material type.<sup>[22]</sup> Popular force fields for MOFs include the universal force field,<sup>[23]</sup> the extension for MOFs,<sup>[24]</sup> the ab initio force field (FF) MOF-FF,<sup>[25]</sup> PTBFF,<sup>[26]</sup> QuickFF,<sup>[27]</sup> and DREIDING.<sup>[28]</sup> The application of statistical mechanics enables the calculation of ensemble properties, such as free energies, from such simulations.<sup>[22]</sup> Sampling is typically performed by Monte Carlo (MC) simulations, which calculate thermodynamic properties via sampling random parts of conformational space.<sup>[29]</sup> Another popular calculation method is molecular dynamics (MD), in which the interatomic forces are calculated and integrated over time to generate a trajectory. While MM-based simulations are able to address very large structures, an upper limit in regard to computing time and effort is still present. A coarse-grained (CG) simulation offers a trade-off between the accuracy of the simulation and computing time. In a CG simulation, two or more atoms are placed together in a single bead that represents a new “atom.” The interaction of these beads creates the CG force field. Popular CG force fields include the MARTINI force field<sup>[30]</sup> or structure-based models.<sup>[17]</sup>

Adequately simulating hierarchical MOF structures requires including several length scales simultaneously and capturing both amorphous and regular aspects. Thus, simulations should investigate large MOF structures composed of many unit cells. However, to date, simulations have mainly focused on only one or a few unit cells with periodic boundary conditions to predict physical properties. Even in the case of MM simulations, the computing effort is very high for simulations of more than 100 000 atoms on timescales exceeding a few tens of nanoseconds. However, there has been substantial progress in sampling and advanced simulation schemes allowing effective sampling and estimating kinetic behavior even on the second timescale.<sup>[31]</sup> Additionally, it is possible to couple QM/MM simulations as multiscale simulations, in which critical parts of the system are described in electronic detail (QM) while other parts are described atomically (MM).<sup>[32]</sup> Figure 3 presents an overview of the simulation techniques and their suitability to specific properties.

Simulations have successfully investigated various interesting properties,<sup>[33]</sup> such as mechanical stabilities under pressure or changing solvent conditions, of MOFs (e.g., MOF-5<sup>[34]</sup>). Here, simulations allowed to pinpoint instabilities arising from MOF-oxygen atom interactions with water and to increase the water stability of MOF-5. Similarly, DFT simulations allowed to investigate mechanical stability and quantify the elastic properties of the material by calculating the shear modulus and Young's modulus.<sup>[35,36]</sup> Other simulations investigated the efficiency of diffusion as determined by the structure and functionalization of a MOF. The simulated adsorption isotherms

of Ar, CH<sub>4</sub>, and H<sub>2</sub> for different MOFs were compared against experimental data within a 10–15% error range.<sup>[37]</sup> Many MOFs (MOF-2, MOF-3, IRMOF-1, IRMOF-6, IRMOF-8 (where IRMOF = isorecticular metal–organic framework)) were found not suitable for hydrogen storage. Storage (mainly of gases) in MOFs by adsorption is closely related to the diffusion of guest molecules through the pores of a MOF. Functionalizing the organic linkers allows MOFs to be adjusted for different applications, e.g., for use as batteries or for energy storage.<sup>[38]</sup> Simulations have shown that by either increasing the aromatic content of the organic linker in Zn-MOF-C6 or changing the Zn to Mg, the hydrogen uptake increased.<sup>[39]</sup> Another application for nanoporous materials such as MOFs is carbon dioxide capture. Ionic liquid (IL)/IRMOF-1 composites are classified as good candidates for CO<sub>2</sub> capture in simulation.<sup>[40]</sup> Gas separation can be achieved by MOFs sensitive to only one type of molecule/atom to filter mixed gases.<sup>[41]</sup> Some MOFs, such as UiO-66 (where UiO = Universitet i Oslo) or HKUST-1 (where HKUST = Hong Kong University of Science and Technology), have different pore sizes and can be used for more complex storage or separation processes, with simulations predicting the dependency on the electrostatic interaction.<sup>[42]</sup> Evaluating the bandgap via DFT allows the determination of the conducting type of the MOF and the identification of novel semiconductors.<sup>[43]</sup> For example, the calculated bandgap of MOF-5 is 2.5 eV, which would classify MOF-5 between insulating and semiconducting materials.<sup>[36]</sup> The thermal conductivity can be determined via MD. For MOF-5, the thermal conductivity is ≈0.31 W (mK)<sup>-1</sup> and is weakly dependent on temperature,<sup>[44]</sup> which classifies MOF-5 as an insulating material. Based on these examples, it appears feasible to extend QM, MM, and multiscale QM/MM simulations beyond these idealized small systems with perfect crystal symmetries to set up realistic hierarchical MOF structures and investigate their properties in greater detail.

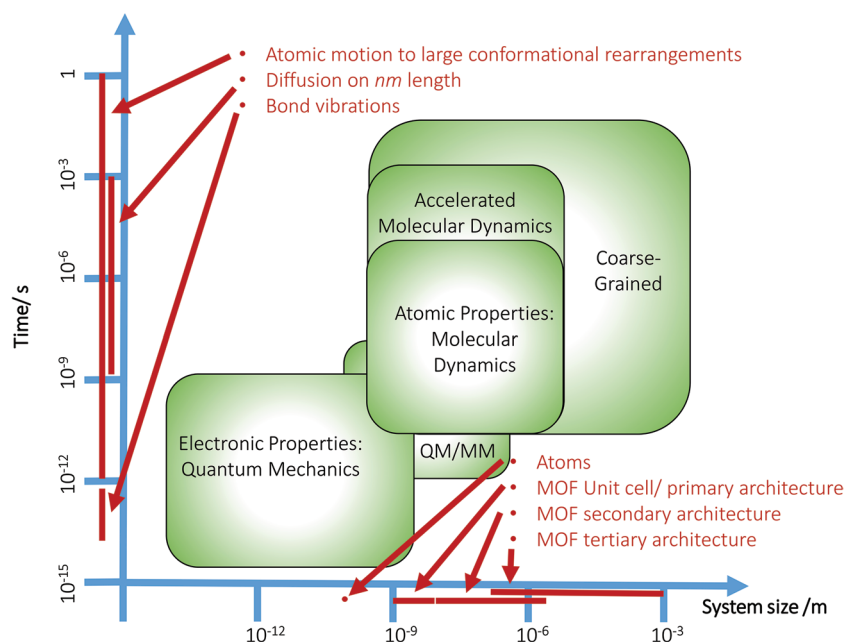


**Figure 3.** Simulation techniques for different time and length scales. Added in red are indicators where particular aspects relevant for MOF and MOF simulations are typically located in time or space.

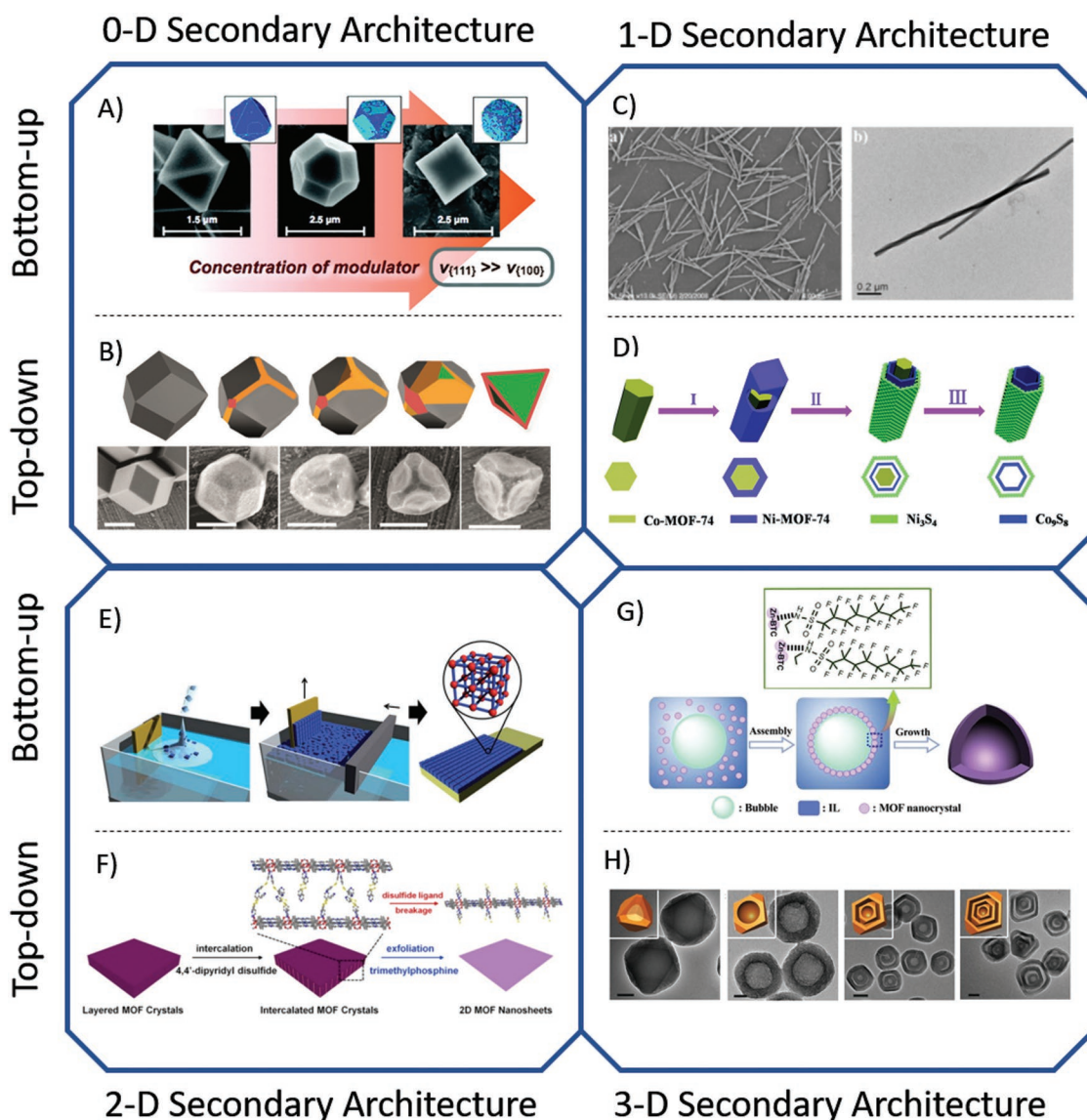


**Figure 4.** A–H) Production of MOFs with secondary hierarchical architecture. A) Reproduced with permission.<sup>[48]</sup> Copyright 2011, American Chemical Society. B) Reproduced with permission.<sup>[49]</sup> Copyright 2015, Wiley-VCH. C) Reproduced with permission.<sup>[50]</sup> Copyright 2011, American Chemical Society. D) Reproduced with permission.<sup>[51]</sup> Copyright 2018, The Royal Society of Chemistry. E) Reproduced with permission.<sup>[75g]</sup> Copyright 2011, American Chemical Society. F) Reproduced with permission.<sup>[53]</sup> Copyright 2017, American Chemical Society. G) Reproduced with permission.<sup>[110]</sup> Copyright 2014 Elsevier. H) Reproduced with permission.<sup>[112]</sup> Copyright 2017 Wiley-VCH.

## 2. MOFs with Hierarchical Architectures

As stated above, the primary hierarchical architecture of a MOF is its crystal structure. In the following section, we will focus on the synthesis and simulation of secondary and higher-order architectures of MOFs.

### 2.1. MOFs with Hierarchical Architectures in Experiments

When constructing a MOF with hierarchical architectures, bottom-up approaches focus on the control of crystallization and growth processes,<sup>[45]</sup> including utilizing templated crystallization, interfacial crystallization, sol-gel processing,<sup>[46]</sup> and metal

template transformation. Besides, top-down approaches mainly include postsynthetic functionalization, chemical etching,<sup>[47]</sup> and delamination processes. However, some processes, such as surface-energy-driven process, can shape MOF crystals at different length scales and thus can be applied in both approaches.

#### 2.1.1. MOFs with Secondary Hierarchical Architectures

A secondary architecture can span different dimensions, leading to 0D, 1D, 2D, and 3D architectures. Apart from the 1D MOF secondary architecture, bottom-up approaches and top-down approaches have been widely used in the construction of these hierarchical architectures (Figure 4).

**MOF 0D Secondary Architecture:** How to control the size and the shape of MOF nanoparticles is vital in constructing MOF 0D secondary architectures. In addition to some cases where templates were employed,<sup>[55]</sup> most approaches have focused on the control of nucleation rate and crystal growth rate. Both microwave and ultrasound can accelerate the nucleation rate and crystal growth rate, helping to produce MOF 0D secondary architectures.<sup>[56]</sup> Modulators such as water,<sup>[57]</sup> methanol,<sup>[58]</sup> acids,<sup>[48,59]</sup> and amine<sup>[60,61]</sup> have also been added to adjust and control the growth of MOF 0D secondary architecture.<sup>[62]</sup>

It is rare to construct MOF 0D secondary architectures via top-down approaches. However, Avci et al. reported the shape modification of MOFs via anisotropic etching. ZIF-8 crystals (where ZIF = zeolitic imidazolate framework) were etched, with their crystal shape changing from rhombic dodecahedron to cubic.<sup>[49]</sup>

**MOF 1D Secondary Architecture:** MOF 1D secondary architectures include nanotubes, nanorods, and nanowires, which are more challenging to produce than MOF 0D secondary architectures.

Bottom-up approaches are widely used in production, such as liquid-phase epitaxy methods, which allow rod-type MOFs to be grown from gold surfaces.<sup>[63]</sup> Modulators can also control the growth of MOFs to form nanorods via solvothermal synthesis<sup>[61]</sup> or the reverse-phase microemulsion technique.<sup>[50]</sup> Recently, Zou et al. reported an amorphous MOF-mediated recrystallization approach to construct single-crystal Co-MOF-74 nanotubes from MOF-74 nanoparticles. In this synthesis approach, amorphous Co-MOF-74 nanoparticles were recrystallized in a water solution at 175 °C to form nanotubes, wherein the nanotube length was largely affected by the pH value.<sup>[64]</sup> Apart from these methods that are designed for specific types of MOFs, templates provide a more general approach. For instance, MOFs can be coated on the surface of insoluble rod-type templates consisting of polymers,<sup>[65]</sup> metal oxides,<sup>[66]</sup> or metal nanowires<sup>[67]</sup> to form 1D secondary architectures. Upon template removal, MOF nanotubes can be formed.<sup>[68]</sup>

With regard to top-down approaches, there are only a few reports on etching to form 1D structures because it is hard to control the etching process or defects inside MOFs.<sup>[69]</sup> However, it has been shown that MOF tubes can be transformed into MOF-shell-type tubes using etching.<sup>[51]</sup>

**MOF 2D Secondary Architecture:** The production of MOF 2D secondary architectures has been widely studied for both bottom-up and top-down approaches.<sup>[69,70]</sup>

Bottom-up approaches include modulated synthesis and interfacial synthesis. By adding acid,<sup>[61,71]</sup> salt,<sup>[72]</sup> or triethylamine<sup>[73]</sup> as modulators during MOF growth, a MOF 2-D secondary architecture can be obtained. Interfacial synthesis has also been investigated using liquid/liquid interfaces<sup>[74]</sup> and gas/liquid interfaces (mainly the Langmuir–Blodgett method).<sup>[52,75]</sup> The production of films at the liquid/gas interfaces leads to monolayer structures, whereas those at liquid/liquid interfaces have minimum thicknesses of ≈100 nm. Apart from interfacial synthesis, MOF thin films can grow within a mixed-solvent layer via interdiffusion of the metal ions and ligands, through which the yield substantially increased.<sup>[76]</sup>

Top-down approaches, such as exfoliating MOF crystals via different processes, are popular methods for the production of MOF 2D secondary architectures: these approaches

include sonication,<sup>[77,78]</sup> mechanical exfoliation,<sup>[78,79]</sup> chemical exfoliation,<sup>[53]</sup> and solvent-induced delamination.<sup>[80]</sup> By taking advantage of the weak interactions or instabilities of linkers<sup>[53,81]</sup> inside MOF structures, crystals can be exfoliated into 2D secondary architectures. In most of these cases, the yield is the major challenge, as the MOF sheet thickness can vary within a certain range and be difficult to control.

Apart from the approaches of construction of nanosheet-type 2D secondary architectures, methods have also been developed for MOF films, layers, and patterned layers,<sup>[82]</sup> most of which have higher thicknesses and extended areas, leading to 2D secondary architecture at a larger scale.

The growth of MOFs on solid surfaces also often leads to MOF thin films. Different methods can be used to produce MOF films or layers on solid surfaces, such as the layer-by-layer (LbL) method,<sup>[83]</sup> substrate-seeded heteroepitaxy,<sup>[84]</sup> electrochemical deposition,<sup>[85]</sup> powder MOF-based deposition,<sup>[86]</sup> atomic layer deposition,<sup>[87]</sup> and chemical vapor deposition.<sup>[88,89]</sup>

Along with the production of MOF layers on solid surfaces, different methods have been applied for MOF patterning on surfaces,<sup>[90]</sup> for instance, inkjet printing,<sup>[91]</sup> scanning-probe assisted patterning,<sup>[92]</sup> and microcontact printing with solvothermal process<sup>[93,94]</sup> or with LbL methods.<sup>[95]</sup> Light has also been applied to structure MOF films via photolithography of the substrate<sup>[95]</sup> or via electron beam lithography.<sup>[96]</sup> Applying an IR laser to locally heat a substrate and confine the MOF growth has also been reported as a promising tool for direct laser writing of MOFs.<sup>[97]</sup> Top-down approaches, which follow partial removal of the MOF layer, have also been reported.<sup>[98]</sup>

**MOF 3D Secondary Architecture:** 3D secondary architectures mainly involve hollow or porous MOFs, which have uneven distributions of MOF materials in 3D space. Some case of MOF 3D secondary architectures contain hierarchical porosity, which will be discussed in more detail in Section 3.

In regard to the construction of hollow MOF architectures, the bottom-up approaches have often been applied using spherical templates.<sup>[99]</sup> Hard templates, such as polystyrene,<sup>[54]</sup> metal oxides,<sup>[100]</sup> alumina,<sup>[101]</sup> or silica spheres,<sup>[102]</sup> are difficult to remove, which often result in the formation of particles with MOF shells. By the partial removal of the hard template, the so-called “yolk–shell” architecture also formed.<sup>[100,103]</sup> Such structures are often applied in batteries.<sup>[104]</sup> Soft templates, such as surfactants<sup>[54,105]</sup> and cell walls,<sup>[106]</sup> can be used in the production of shell-type MOF architectures.

MOF 3D secondary architectures can also be produced by interfacial synthesis.<sup>[107]</sup> Spray-drying of a MOF precursor solution leads to crystallization at the gas–liquid interface<sup>[108]</sup> and the formation of oil drops in aqueous solutions can template the crystallization at such liquid–liquid interface.<sup>[109]</sup> Additionally, gas bubbles can be used as templates to produce hollow MOF architecture.<sup>[110]</sup>

Top-down approaches, mostly involving etching, have also been used in MOF production.<sup>[111]</sup> Taking advantage of surface-energy-driven mechanisms, MIL-101 (where MIL = Matériaux de l'Institut Lavoisier) growth and etching with acetic acid lead to a multishelled hollow MOF architecture.<sup>[112]</sup>

To build MOF 3D architectures at larger length scales, one method is to construct a 3D structure for a different material and later mix or coat the structure with MOFs.<sup>[113]</sup> MOF hollow

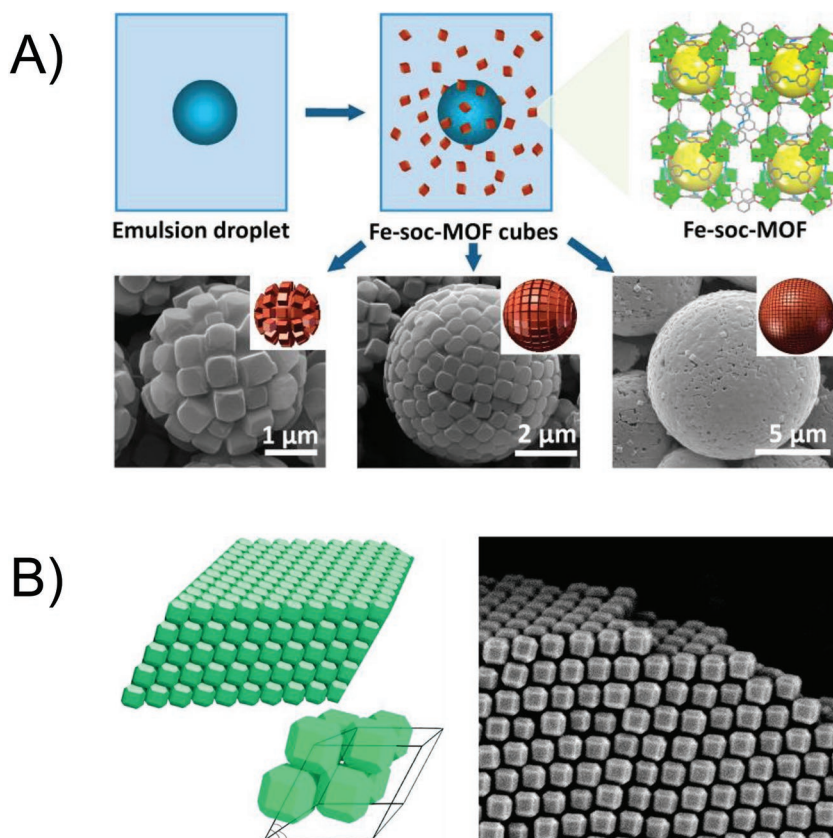


**Figure 5.** A) Self-assembled superstructure of ZIF-8 and its simulation. Reproduced with permission.<sup>[118]</sup> Copyright 2013, American Chemical Society. B) FE-SEM image and simulation of ZIF-8 superstructure. Reproduced with permission.<sup>[119]</sup> Copyright 2017, Nature Publishing Group.

tubes have been obtained by mixing UiO-66 or ZIF-8 with sodium alginate.<sup>[114]</sup> In addition, 3D printing has been applied in the construction of acrylonitrile butadiene styrene frameworks coated with copper benzene-1,3,5-tricarboxylate.<sup>[115]</sup>

### 2.1.2. MOFs with Tertiary Hierarchical Architectures

Assembling MOF secondary hierarchical architectures can lead to MOF tertiary architectures. Through the seeding process<sup>[116]</sup> or linear assembly,<sup>[117]</sup> MOF particles with defined 0D secondary hierarchical architectures can create a 1D tertiary architecture. Similar strategies can be used for the construction of MOF 3D tertiary architectures. By applying soft template methods using

colloidosomes, MOFs with triple hierarchical architectures can be formed via Pickering emulsion.<sup>[118]</sup> In this hollow architecture, different levels of hierarchical architecture can be easily observed. The Fe-soc-MOF lattices, as primary architectures, form defined cubic particles as secondary architectures, which then gather into shell-type tertiary architectures. Avci et al. recently reported the self-assembly of truncated rhombic dodecahedral particles of ZIF-8 into millimeter-sized tertiary hierarchical architectures<sup>[119]</sup> (Figure 5).

MOF 2D secondary hierarchical architectures can also be assembled. A nickel-based MOF with a 2D secondary hierarchical architecture, for instance, can form an accordion-like tertiary hierarchical architecture through ultrasonication; this MOF exhibited an excellent electrochemical performance.<sup>[120]</sup> Recently, Tan and Zeng reported the synthesis of HKUST-1 with three orders of hierarchical architectures, where the layered MOFs form a ring-like tertiary hierarchical architecture. They proposed a template-assisted growth mechanism, which shows the great potential of template methods for the synthesis of hierarchical MOFs (Figure 6).<sup>[121]</sup>

Additionally, liquid-phase epitaxy methods on selected substrates can produce MOFs with tertiary hierarchical architectures. Falcaro et al.<sup>[122]</sup> reported growing MOFs on the substrate of crystalline copper hydroxide to obtain film-type tertiary hierarchical architectures with particle-type secondary hierar-

chical architectures.

By combining bottom-up and top-down approaches, tertiary hierarchical architectures can be prepared. By etching<sup>[123]</sup> or substitution,<sup>[12]</sup> shell-type structures of MOF crystals can be realized (Figure 7). Additionally, anisotropically etching ZIF-8 and ZIF-67 with xylenol orange under the control of pH value leads to hollow-box-shaped or concave-tetrahedron-shaped MOF nanoparticles.<sup>[124]</sup>

### 2.2. MOFs with Hierarchical Architectures in Simulations

Simulations of the primary hierarchical architectures (i.e., the crystal structure) of many different types of MOFs, such as

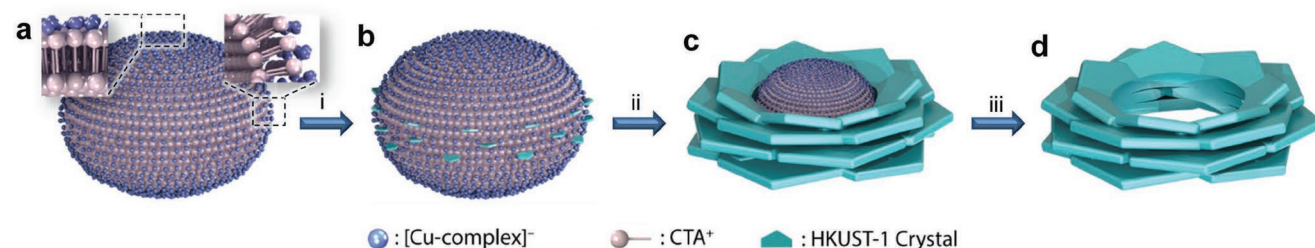


**Figure 6.** HKUST-1 with ring-like tertiary hierarchical architecture. Reproduced with permission.<sup>[121]</sup> Copyright 2017, Wiley-VCH.

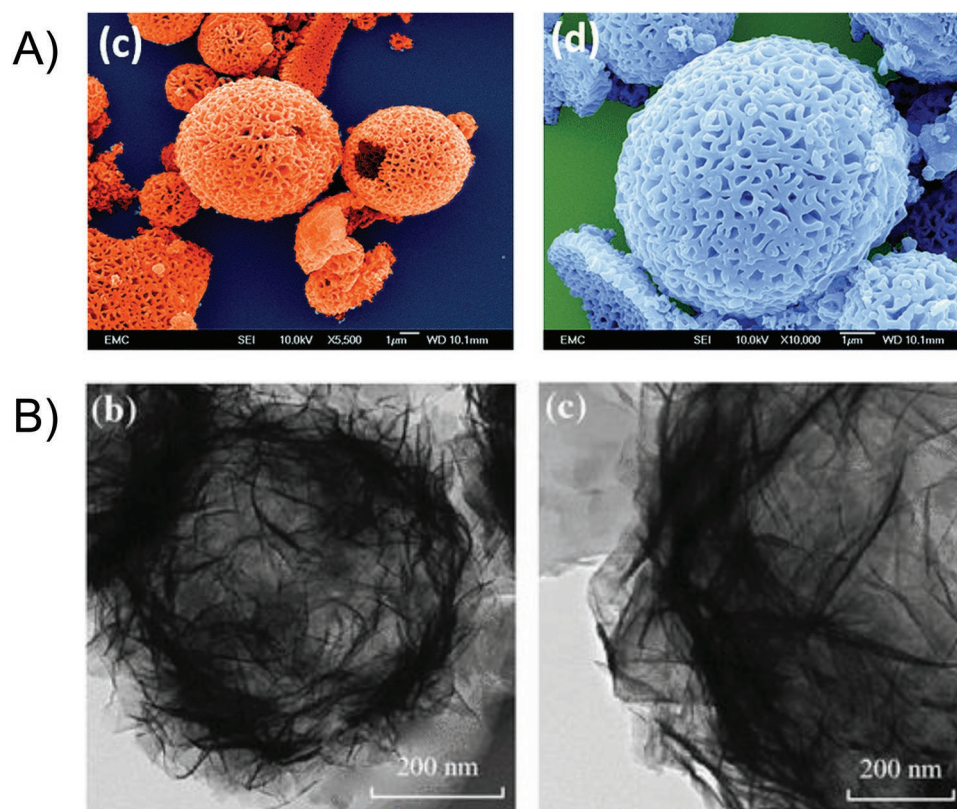


**Figure 7.** A) Etching for ZIF-8 hollow structure for formation of higher hierarchical structure. Reproduced with permission.<sup>[123]</sup> Copyright 2018, The Royal Society of Chemistry. B) Transformation and substitution of ZIF-8 lead to the 2D hollow MOF nanoflake spherical microstructures. Reproduced under the terms of the CC-BY Creative Commons Attribution 4.0 International License (<http://creativecommons.org/licenses/by/4.0/>).<sup>[12]</sup> Copyright 2017, The Authors, published by Springer.

MOF-5, UiO-66, and HKUST-1, have already been reviewed several times as elaborated in the introduction. Here, we will focus on simulating secondary hierarchical architectures. The secondary hierarchical architectures of MOFs describe the morphology of a material. Knowing the shape of a MOF crystal is essential to use it as a building block for future applications.

### 2.2.1. Secondary Hierarchical Architectures

Umemura et al. investigated the morphology of the HKUST-1 framework by doing MC simulations using the coordination modulator method with lauric acid as a modulator.<sup>[48]</sup> The goal was to examine the correlation between the modulator concentration and the framework morphology (Figure 8). The growth probability (and dissolution probability) of each site of the framework was calculated by using the Gibbs free energy of the respective site. Hence, faces (100) and (111) were expected to dominate the growth mechanism. The relative energies between those sites determined the growth and finally the morphology. For example, a larger relative energy for the (100) face than for the (111) face resulted in an octahedral morphology, and a much larger relative energy of the (111) face led to a cubic morphology. In this example, the simulation showed that regulating the relative energies by changing the modulator concentration was responsible for the different morphologies

of the crystal. The study also showed that the contribution of the btc ligand plays a vital role in crystal growth, as the (100) site needs only six btc ligands to contribute to the formation of the cuboctahedron, and in contrast, the (111) site needs eight btc ligands. Adding monocarboxylic acid as a modulator perturbs the attachment of the growth unit because the modulator and a carboxylate in the btc ligand compete with each other at the attachment event. The results of the study concluded that changing the modulator concentration generates a perturbation in the growth process that leads to a larger impact on the (111) site because this site possesses more btc ligands and thus more competing carboxylates, which results in a change in relative energies and subsequently explains the crystal morphology transition.

A similar but more general approach was used by Anderson et al. where not only MOFs but also zeolites and other materials were examined.<sup>[125]</sup> In this study, coarse graining was realized by partitioning the crystal structure with nodes at the metal clusters and edges of the tiles at the linkers. These partitions represented the Miller planes as in the study above and were used to grow the crystals. The growth of the crystals also followed the same MC method, where the probabilities for crystal growth and dissolution were derived from the Gibbs free energy. The frameworks of HKUST-1 and MOF-5 were successfully simulated and agreed with the experimental results.



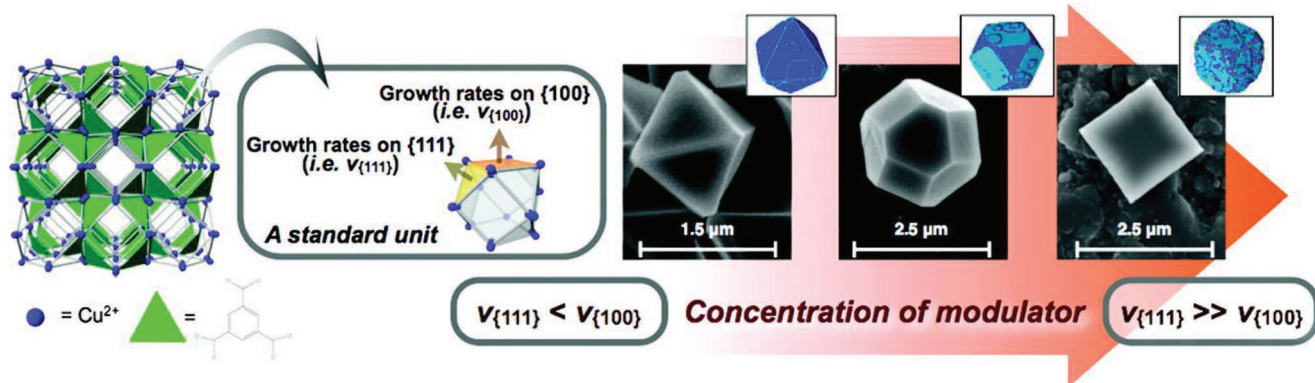


**Figure 8.** Changing the modulator concentration transitions the morphological shape of HKUST-1 from an octahedron to a cube. Reproduced with permission.<sup>[48]</sup> Copyright 2011, American Chemical Society.

### 2.2.2. Tertiary Hierarchical Architecture

A tertiary hierarchical architecture is composed of many building blocks with defined morphologies on a smaller length scale, i.e., the secondary hierarchical architecture. Having access to a collection of many MOF crystals with diverse morphologies enables tailored macro materials for a given application. The next step would obviously be to control the tertiary hierarchical architecture, where many building blocks come together to build a macroscopic material, by setting up a CG model that describes the interaction of the building blocks. The interactions of the building blocks with neighboring building blocks can be estimated from initial all-atom simulations to simulate large-scale tertiary hierarchical MOF architectures.

One possibility to generate tertiary hierarchical architectures is to use the floppy-box MC method, where the macroscopic structure is constructed by self-assembly of the building blocks from the secondary hierarchical architecture. In this method, the alignment of the building blocks, which represent secondary hierarchical structures, comes from increasing the pressure of the simulation box to obtain the densest packings containing all three forms of hierarchical architecture. A study by Maspoeh and co-workers confirmed the good agreement of this method with experimental results for ZIF-8 and UiO-66.<sup>[119]</sup>

## 3. MOFs with Hierarchical Porosities

There are two kinds of MOF materials with hierarchical porosities. One is an all-MOF material with multiple scales of porosity, which is the main focus in this section. Another kind of hierarchically porous material can be achieved by combining MOF with another material that is usually mesoporous or macroporous to create hybrid structures, wherein MOFs usually provide microporosity. Following this approach, several hierarchically porous materials have been constructed and applied.<sup>[89,126]</sup>

### 3.1. MOFs with Hierarchical Porosities in Experiments

Analogous to MOF hierarchical architectures, the primary hierarchical porosity of a MOF is its intrinsic microporosity originating

from the framework. To generate hierarchically porous all-MOF materials, higher orders of hierarchical porosity have to be generated in the mesoporous or macroporous range, where both bottom-up and top-down approaches have been developed.

#### 3.1.1. Bottom-Up Approaches

Inspired by traditional zeolites with hierarchical structures, template strategies, with both soft and hard templates, have become a widely used method in the production of MOFs with hierarchical porosity.<sup>[127]</sup>

Soft template methods involve the self-assembly of structure-directing agents (SDAs) to form a template and the interaction of SDAs with metal ions or linkers to control MOF growth. Different surfactants, which involve cationic SDAs, anionic SDAs, organic amines, and polymers, have been used for soft template formation, such as cetyltrimethyl ammonium bromide (CTAB),<sup>[128]</sup> cetyltrimethylammonium chloride,<sup>[94,129]</sup> amphiphilic dodecanoic acid,<sup>[130]</sup> N,N-dimethyloctadecylamine,<sup>[131]</sup> and nonionic block copolymers.<sup>[132]</sup> Several small molecules, such as 1,3,5-trimethylbenzene<sup>[128]</sup> and citric acid,<sup>[133]</sup> have been applied to adjust the formation of the template and the nanocrystals. By combining CTAB as a template with the electrochemically assisted self-assembly technique, MOF thin films have been grown on electrodes with 2D honeycomb-like mesopores as secondary hierarchical porosities in the walls of the cavities.<sup>[134]</sup> Recently, by using highly ordered polystyrene (PS) monoliths as a template, a single crystal with oriented and ordered macropores and micropores has been prepared.<sup>[135]</sup>

Hierarchically porous MOFs with micropores and mesopores as secondary hierarchical porosities can also be produced by combining ILs, supercritical carbon dioxide (scCO<sub>2</sub>), and surfactants to form emulsion systems.<sup>[136]</sup> Additionally, the production of MOFs with CO<sub>2</sub>-expanded dimethylformamide can introduce secondary hierarchical porosity in a structure.<sup>[137]</sup>

For the production of higher orders of hierarchical porosity, Reboul et al.<sup>[138]</sup> reported metal templates, such as hexagonal patterns and aerogels of alumina, that were transformed into hierarchically porous MOFs via reaction with linkers, resulting in MOFs containing micropores, mesopores, and macropores (Figure 9).

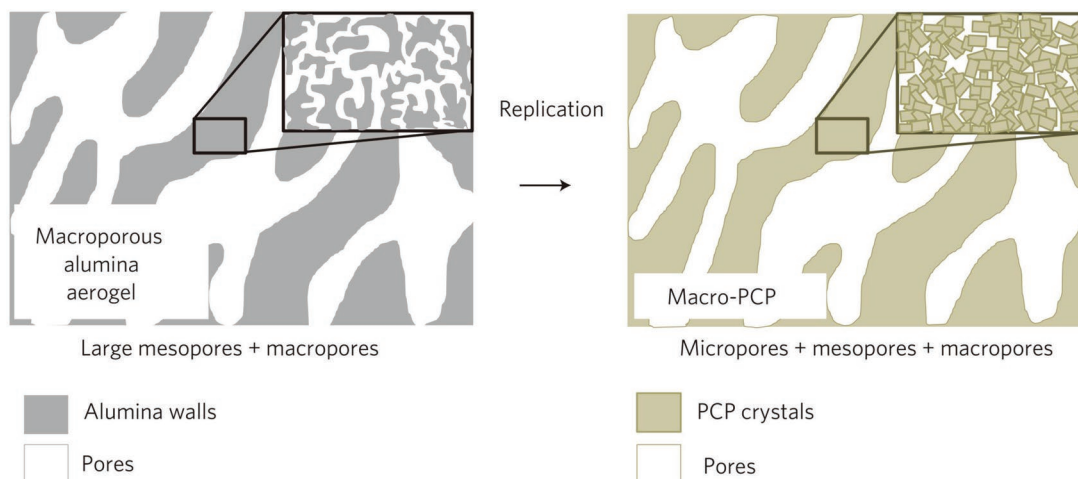


**Figure 9.** Hierarchically porous MOF materials with three levels of porosity. Reproduced with permission.<sup>[138]</sup> Copyright 2012, Nature Publishing Group.

### 3.1.2. Top-Down Approaches

Top-down approaches have mainly focused on the introduction of structural defects and partial removal of metal nodes or linkers within MOFs. Taking advantage of coordination bonds inside MOFs, controlled treatment with water,<sup>[139]</sup> acid,<sup>[140]</sup> or  $H_2O_2$ <sup>[141]</sup> will partially destroy the MOF structure, leading to hierarchical porosity (**Figure 10**).

Zhang et al.<sup>[142]</sup> reported an etching method to produce MOFs, where they controlled the size, shape, and space

distribution by using nanoparticles as a hard template. After Au nanoparticles were encapsulated into ZIF-8 with following etching in solution of KI and  $I_2$ , MOFs with secondary hierarchical porosities in the mesoporous range were prepared, which maintained a good crystal structure. Recently, Meng et al.<sup>[143]</sup> reported a method to introduce secondary hierarchical porosities into MOFs by annealing nanoparticles@MOFs at an appropriate temperature. Taking advantage of the low thermal stabilities of defects at the connections of the MOF and nanoparticles, the annealing process

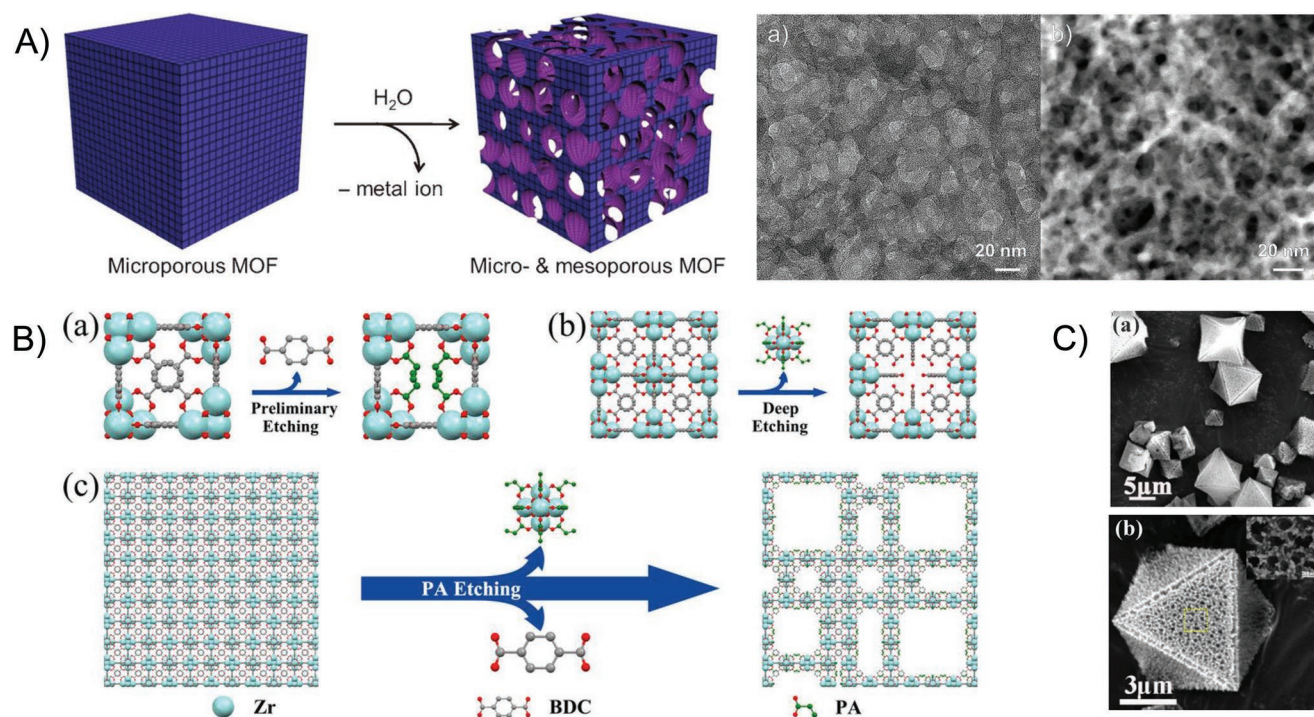


**Figure 10.** A) POST-66(Y) was treated with water. Reproduced with permission.<sup>[139]</sup> Copyright 2015, Wiley-VCH. B) UiO-66 was treated with acid. Reproduced with permission.<sup>[140]</sup> Copyright 2018, Wiley-VCH. C) Cu-TATAB framework was treated with  $H_2O_2$ . Reproduced with permission.<sup>[141]</sup> Copyright 2018, Elsevier.

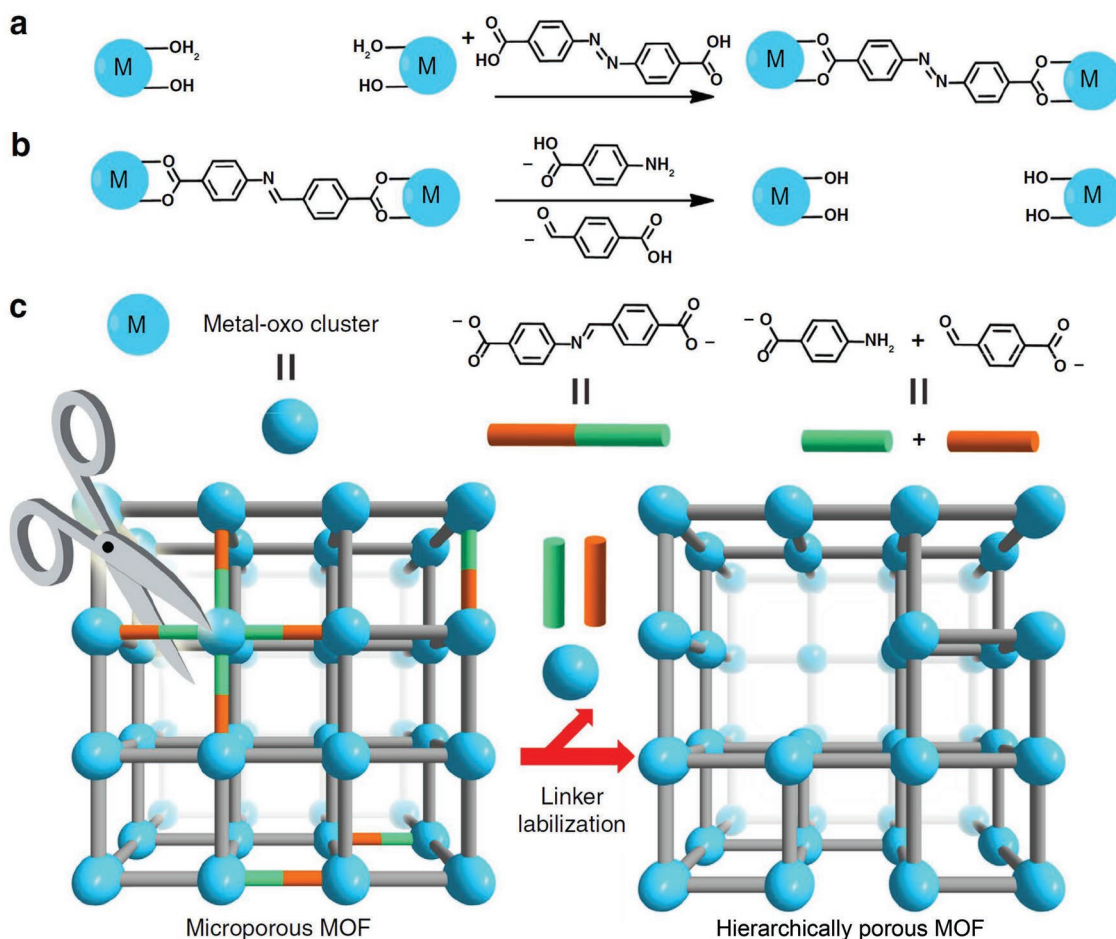


**Figure 11.** Formation of secondary porosity through instability of MOF linkers. Reproduced under the terms of the CC-BY Creative Commons Attribution 4.0 International License<sup>[144]</sup> Copyright 2016, The Authors, published by Springer Nature.

destroyed these areas, which introduced secondary hierarchical porosity in the material.

However, controlling the partial removal of MOF segments from the structure can be challenging, and this removal sometimes leads to total decomposition of the primary porosity. An alternative strategy is the introduction of unstable linkers into MOFs.<sup>[144]</sup> PCN-160 with azobenzene-4,4'-dicarboxylate as a linker was synthesized and exchanged by 4-carboxybenzylidene-4-aminobenzoate, which can be cleaved via a one-step hydrolysis reaction. After the conditions for synthesis, exchange, and acid treatment were carefully chosen, hierarchically porous MOFs were obtained (Figure 11).

### 3.2. MOFs with Hierarchical Porosities in Simulations

Metal nodes and linkers in the crystal structure create large empty pockets that result in the primary porosity of a MOF. This primary porosity of a MOF has been frequently computationally researched, and MD simulations on diffusion, gas storage, and gas separation of the primary hierarchical porosity are quite common.<sup>[145]</sup>

#### 3.2.1. Secondary Hierarchical Porosity

The next step would be to perform these simulations including the secondary hierarchical porosity. The technique to investigate these structures through MD simulations differs from the previous simulation, where only the primary hierarchical porosity was regarded. The first issue is to generate a proper structure with mesopores. A study by Dürholt et al. applied a CG force field on HKUST-1, wherein metal nodes and linkers were represented as single beads.<sup>[146]</sup> The reason for choosing a CG model is the scale of the simulation. A mesopore can be several nanometers in size, and a system containing many such pores results in a large-scale bulk material. An atomistic representation of the structure would therefore result in very long computing times.

The interactions between the simplified beads, representing the metal nodes and linkers, were derived from the MOF-FF force field. Mesopores were cut out spherically (to reduce computing effort), and the open ends were removed or saturated with methyl groups, depending on the bonding type. After the simulation, the structure was transferred back to the atomistic representation and the orientation of the building blocks was then corrected (Figure 12).

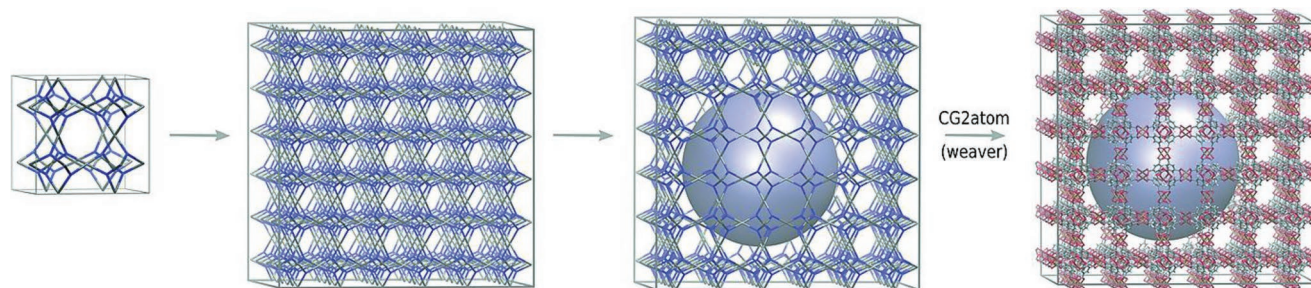


**Figure 12.** The first step of the multiscale simulation is to create a supercell and a spherical mesopore is cut out. An optimization is executed by applying a coarse-grained force field to the structure. Analysis of the simulation is performed after returning to the atomistic representation. Reproduced with permission.<sup>[146]</sup> Copyright 2016, Wiley-VCH.

The goal was to determine the relationship between the structural and mechanical properties depending on the size of the mesopores, i.e., the secondary hierarchical porosity. The calculated bulk modulus decreased with increasing mesopore size, and the overall hierarchical structure with few large mesopores was more stable than the hierarchical structure with more small mesopores.

The study by Fang et al. examined the role of defects in MOFs.<sup>[32]</sup> In this study, the defects originated from modified linkers, which replaced the standard linker of the HKUST-1 framework. The structure itself was simulated by applying the MOF-FF force field, whereas a single defective linker and its related paddlewheel were calculated separately with DFT calculations. The defect degree was defined by the type of functional group within the modified linkers (**Figure 13**). It was found that changing the electronic structure of the MOF by introducing defects changes the behavior of the material, such as developing a tendency toward reduction. The results can then be further used to calculate/predict other physical properties, such as magnetism and conductivity.

### 3.2.2. Tertiary Hierarchical Porosity

Simulation of higher order hierarchical porosity within MOFs has not been done so far. To simulate, for example, a tertiary hierarchical porosity, one could follow the same procedures as described for the secondary hierarchical porosity in a way that generates macropores (Figure 9). Computational challenges would be creating input files for the simulation. The structure itself could be generated by using the data from the simulations of secondary hierarchical porosity as building blocks for the

tertiary structure. For example, expanding the secondary structure and then randomly removing some building blocks could generate those macropores. Furthermore, a CG model similar to the one used in the work of Dürholt et al.<sup>[146]</sup> that describes a building block (and not a node/linker) could be used. The drawback of this method is that the simulation would not be able to show the effect of every type of porosity in a single simulation where atomistic detail is required, such as the breathing capabilities of MOFs. Breathing of a MOF comes from synergetic effects of coordination chemistry between metal nodes and linkers and results in an increase or decrease of pore sizes,<sup>[147]</sup> whereas guest molecules also play a vital role. But simplifying the crystal structure by a CG model would result in a lower resolution of the model, atomistic effects would then not be visible.

## 4. MOFs with Hierarchical Compositions

MOFs are composed of metal nodes connected by organic linkers that are structured at a molecular level within the framework, which is regarded as the primary hierarchical composition. Structuring different components within selected regions in one MOF crystal or within different layers of a MOF film at a microscopic or macroscopic length scale leads to a secondary composition.

### 4.1. MOFs with Hierarchical Compositions in Experiments

To produce MOFs with hierarchical compositions, liquid-phase epitaxy methods such as seeding or LbL processes are usually applied.

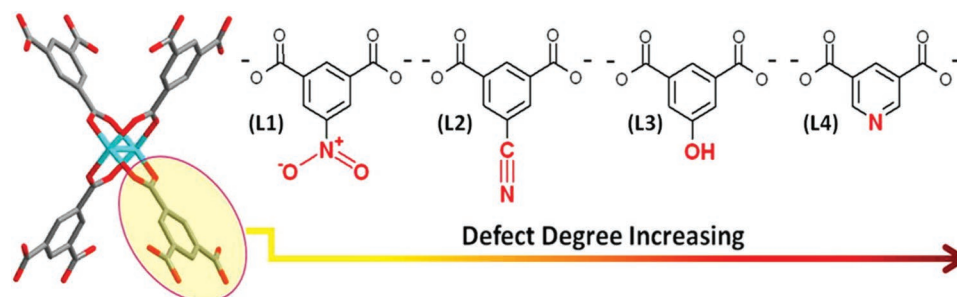


**Figure 13.** The paddlewheel structure is displayed, where one linker is changed by a functional group to generate the defect. The defect degree can be varied by using different functional groups. Reproduced with permission.<sup>[32]</sup> Copyright 2014, American Chemical Society.

**Table 2.** Core–shell-type MOFs with hierarchical composition.

Primary composition (seed)	Secondary composition (shell)	References	Remark
MIL-101(Cr)	UiO-66(Zr)	[149]	–
IRMOF-3; IRMOF-3	MOF-5; IRMOF-3	[10,150]	MOF-5(2nd layer)@IRMOF-3(1st layer)@MOF-5(core), IRMOF-3(2nd layer)@MOF-5(1st layer)@IRMOF-3(core) was also produced
Fe-MIL-88B	Ga-MIL-88B	[151]	–
bio-MOF-11/14	bio-MOF-14	[152]	–
IRMOF-9	Zn <sub>4</sub> O(azbpdC) <sub>3</sub>	[153]	(azbpdC: azide-tagged biphenyl-4,4'-dicarboxylic acid)
UiO-66	NH <sub>2</sub> -UiO-66	[154]	–
Zn <sub>2</sub> (adc) <sub>2</sub> (dabco)	Zn <sub>2</sub> (NH <sub>2</sub> -bdc)(dabco)	[155]	(adc: 9,10-anthracene dicarboxylate; dabco: 1,4-diazabicyclo[2.2.2]octane; NH <sub>2</sub> -bdc: 2-amino-1,4-benzenedicarboxylate)
Co-MOF-74	Ni-MOF-74	[51]	–
UiO-66, Pd-UiO-NH <sub>2</sub>	ZIF-8	[156]	–
IRMOF-1	IRMOF-3	[157]	–
ZIF-8	ZIF-67	[158]	–

#### 4.1.1. Seeding Processes

The seeding process is a classical bottom-up approach to produce layered crystalline materials,<sup>[148]</sup> through which block MOF and core–shell MOF structures can be obtained.

By using a MOF crystal as a seed, an additional MOF of different composition can be grown to obtain core–shell-type hierarchically composed MOFs (Table 2). The core–shell structures represent the secondary composition. For characterization of this kind of MOF, X-ray diffraction and scanning electron microscopy were used. In some cases, different levels of hierarchical composition can be directly observed by optical microscopy.<sup>[10]</sup>

The hybridization of two MOFs is highly dependent on the structures of the MOFs. When Fe-MIL-88B was used as a seed with Ga-MIL-88B was used as the second layer, a core–shell

structure was created. However, when In-MIL-88B was used as the second layer, a block-type structure was obtained. The growth between an isotropic or anisotropic fashion was affected by the crystal lattices of MOFs. By careful selection of the lengths of the linkers, the additional hierarchical composition can be selectively grown on the specific surface. Kitagawa and co-workers<sup>[9]</sup> reported that, with the [Zn<sub>2</sub>(ndc)<sub>2</sub>(dabco)] (ndc: 1,4-naphthalene dicarboxylate) as the primary hierarchical composition, the growth of the [Zn<sub>2</sub>(ndc)<sub>2</sub>(dpndi)] as the secondary hierarchical composition is face-selective (Figure 14).

Comparing core–shell with Janus-type particles, the study by Szilágyi et al. reported that Janus particles do not display any effect of strain, whereas the core of fully coated core–shell particles collapsed upon the formation of the outer shell. Therefore, in such cases the primary hierarchical composition is partially lost.<sup>[159]</sup>

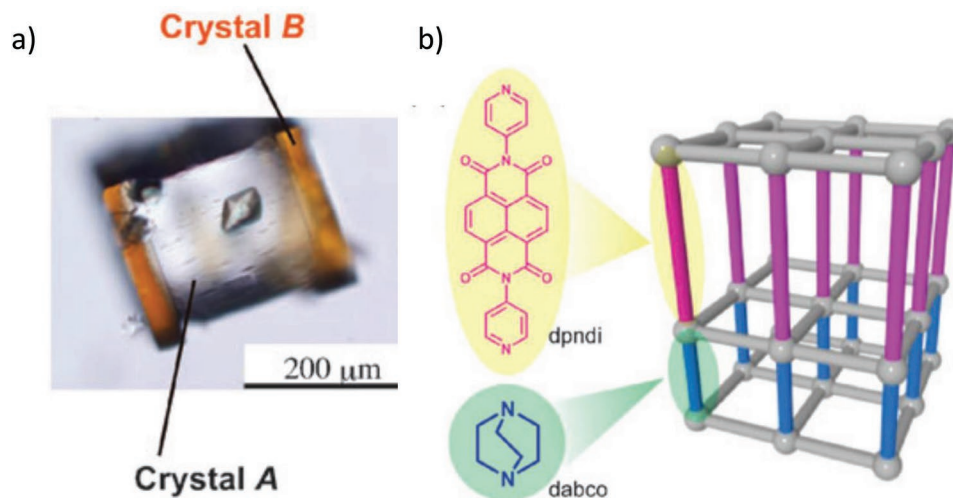


**Figure 14.** a) Face-selective epitaxial growth of MOFs with hierarchical composition. b) Schematic representation and chemical structure of the different linkers in the hierarchical composition. Reproduced with permission.<sup>[9]</sup> Copyright 2009, The Royal Society of Chemistry.

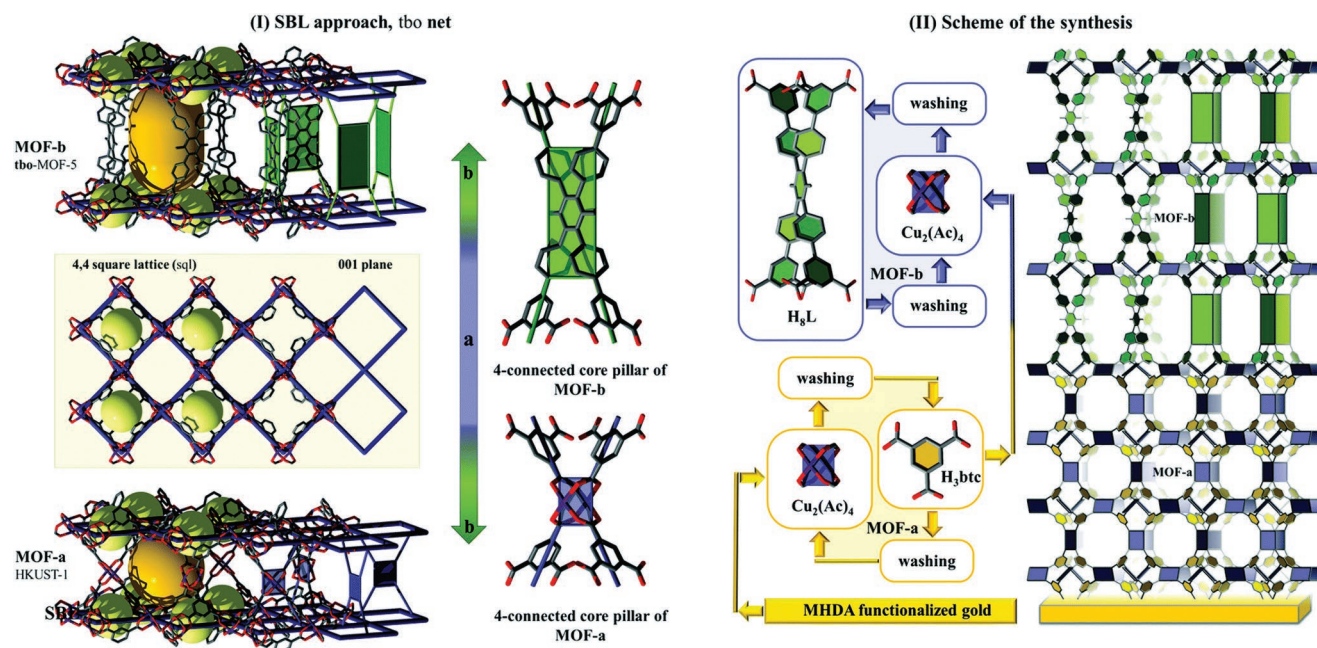


Figure 15. Cu-tbo-MOF-5 was grown on the HKUST-1. Reproduced with permission.<sup>[168]</sup> Copyright 2017, The Royal Society of Chemistry.

#### 4.1.2. Layer-by-Layer Processes

The LbL processes have been widely used in the deposition of MOFs onto flat surfaces or nanoparticles using different techniques, such as spin coating, dipping, and spraying.<sup>[160]</sup> Surface-anchored MOFs with hierarchical compositions have been produced since 2011.<sup>[161,162]</sup> Unlike seeding processes, MOFs with *pcu* topology, such as  $[\text{Cu}_2(\text{ndc})(\text{N,N-ligand})]$ ,<sup>[161–165]</sup>  $[\text{Cu}_2(\text{bdc})(\text{N,N-ligand})]$ <sup>[163,165,166]</sup> (bdc: 1,4-benzenedicarboxylate), and  $[\text{Cu}_2(\text{bpdc})(\text{N,N-ligand})]$ <sup>[165,167]</sup> (bpdc: biphenyl-4,4'-dicarboxylic acid) are preferred in most production processes. Recently, Chernikova et al.<sup>[168]</sup> reported a MOF-on-MOF thin film with a hierarchical composition, where Cu-tbo-MOF-5 was grown on HKUST-1 via the LbL process (Figure 15).

As a substrate for the LbL methods, flat surfaces are usually used, but nanoparticles have also been utilized. With multiple growths on a single magnetic core particle with different types of MOFs via the LbL method, a shell-on-shell-type hierarchical composition was obtained and can be further transformed

into magGEL capsules, inside which cargo molecules can be released at different release kinetics depending on the pH of the environment<sup>[169]</sup> (Figure 16). MOF crystal particles can be used as a surface for other MOF growths through the LbL process, where UiO-66-NH<sub>2</sub> is surrounded by ZIF-8.<sup>[170]</sup>

#### 4.1.3. Others

In addition to these bottom-up approaches, MOFs with hierarchical compositions can be obtained via top-down approaches. Through postsynthetic modification of linkers, portions of the linkers in the crystal can be further transformed to form MOFs with hierarchical compositions.<sup>[171]</sup> Core-shell structures can be obtained from postsynthetic exchange with linker exchange in MOF-5, UCMCM-8 (where UCMCM = University of Michigan Crystalline Material), and UiO-66.<sup>[172]</sup> Additionally, MOFs can change their shapes to obtain hierarchical compositions by ligand exchange. Through treatment with 2-methylimidazole, MOF-5 can be transformed into core-shell-type ZIF-8.<sup>[173]</sup>

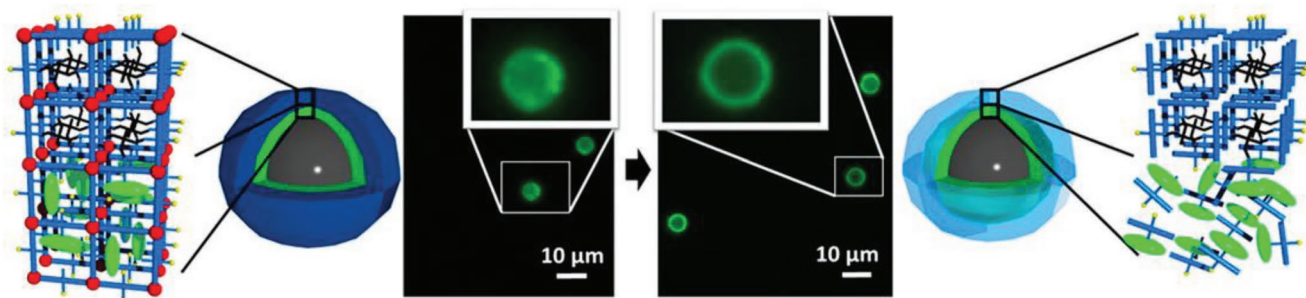
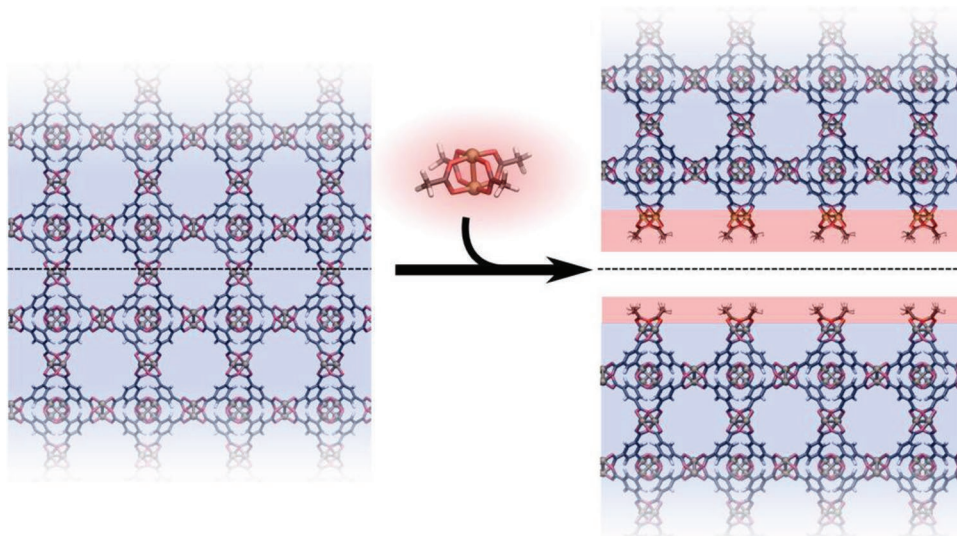


Figure 16. Shell-on-shell MOFs particle and the transformation into magGEL capsules. Reproduced with permission.<sup>[169]</sup> Copyright 2015, American Chemical Society.



**Figure 17.** The structure is sliced into two identical surfaces. A reservoir of  $\text{Cu}_2(\text{Oac})_4$  precursor molecules provides the necessary groups for the saturation. Reproduced with permission.<sup>[176]</sup> Copyright 2014, American Chemical Society.

A hierarchically compositional component with an amide group can be further functionalized.<sup>[161,163,166]</sup> Similarly, a hierarchically compositional component with an azobenzene structure can change its spatial configuration when illuminated.<sup>[166]</sup>

Though epitaxy methods make it possible to construct many MOFs with hierarchical structures, it is hard to hybridize MOFs with different crystallographic parameters. Gu et al.<sup>[174]</sup> overcame these obstacles by introducing polyvinylpyrrolidone as the SDA. They constructed  $\text{NH}_2\text{-MIL-125}(\text{Ti})$  on  $\text{NH}_2\text{-UiO-66}(\text{Zr})$ , which have different morphologies and crystal structures, to obtain a MOF-on-MOF heterostructure as MOFs with hierarchical compositions.

#### 4.2. MOFs with Hierarchical Compositions in Simulations

A single crystal consists of linkers and metal nodes that periodically create the whole structure and thus represents the primary composition. As shown above, this type of hierarchical composition is commonly investigated computationally. The next step toward a higher order hierarchy is to combine different types of MOFs into one crystal, for example, by alternating the linkers (Figure 14b).

##### 4.2.1. Secondary Hierarchical Composition

A simple way to generate a secondary hierarchical composition is to use a graph-based method, wherein the vertices are the metal nodes and the edges represent alternating linkers. An additional advantage of this method is the possibility of freely changing the linkers and can be realized, for example by using the software AuToGraFS.<sup>[175]</sup>

Another method is to connect two MOF crystals at their surfaces. For this approach, the surface properties must be known. The study by Amirjalayer et al. investigated the surface of the

MOF HKUST-1 by cutting it in different Miller planes.<sup>[176]</sup> The open bonds were then saturated by groups taken from a reservoir of  $\text{Cu}_2(\text{Oac})_4$  ( $\text{Oac} = \text{CH}_3\text{CO}$ ) precursor molecules. The surface energy was calculated to find the optimal cutting plane with the minimal difference. Splitting the least number of bonds in a certain Miller plane was important so that the least number of terminating groups was used, which minimized the energy differences (Figure 17). It was concluded that cutting the (111) plane and saturating the remaining open bonds would produce the most stable surface, as the experiments have already shown. Crystal morphology becomes a major point in this method, as cutting different Miller planes results in different morphologies.

A different project by Semino et al. researched the interface between HKUST-1 and a polymer poly(vinyl alcohol) (PVOH) in an atomistic and CG model.<sup>[177]</sup> The interface was produced by combining the acetate terminated (111) plane of HKUST-1 with PVOH. HKUST-1 was modeled with the ab initio force field MOF-FF, and PVOH was described with Chemistry at Harvard Macromolecular Mechanics (CHARMM) (Figure 18). Several equilibrating cycles were performed to stabilize the system. Now, as the next step toward a larger length scale, a new CG model was developed to describe the whole structure, which could be cross-checked with the atomistic data. Subsequently, the density profile, radial distribution functions, and gyration radius for PVOH were calculated for comparison. The problem of the polymer penetrating too deep into the MOF was corrected by tuning the Buckingham potential terms for the polymer. The study confirmed a very good MOF/polymer affinity as a result of strong intermolecular bonds.

Tarzia et al. performed a study to determine the most suitable MOF structures for heteroepitaxial growth on a  $\text{Cu}(\text{OH})_2$  substrate.<sup>[178]</sup> A high-throughput screening of existing MOF databases, such as the computation-ready experimental MOF database, was implemented. The screening process was divided into three major steps. The first step was to investigate MOFs with

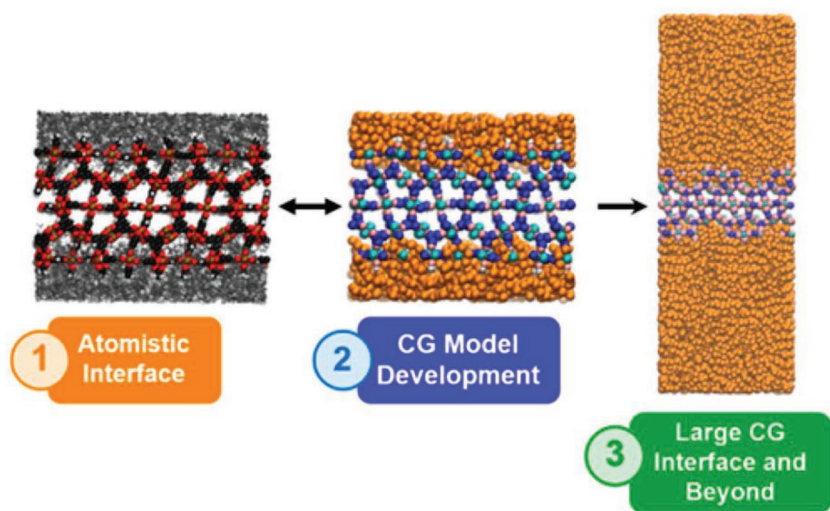


**Figure 18.** Atomistic and coarse-grained representation of the HKUST-1 and PVOH interface. Reproduced with permission.<sup>[177]</sup> Copyright 2017, American Chemical Society.

copper as a metal ion and carboxylate functional groups with each oxygen bound to a copper atom. Two lattice vectors are reduced to create a unique cell called a supercell. In the second step, the passed MOF structures were examined by finding matching supercells of the MOFs to the supercell of the substrate. The MOFs were sliced in different Miller planes to take all resulting supercells into account for the comparison. The assumed most stable way to slice the MOF was to break the least number of bonds. The third and final step of the screening process compared the remaining MOFs to find the ones with the

most favorable binding to the substrate. To do this, the MOF on the substrate–MOF interface was translated in one direction using the MC method to find the optimal position, which was defined by a quantitative relation between binding atoms in each surface and bond pairs in the interface (**Figure 19**). With this method, the screening of the databases resulted in seven experimentally realized MOF structures (i.e., ZAZBUZ). However, in this study, the kinetic and thermodynamic properties of the MOF candidates were not taken into account, and all final candidates possessed at least one plane with rectangular symmetry. This emphasized the expandability of the screening algorithm to not only focus on copper as a metal ion or look only at structures with rectangular symmetry. The study showed the strong influence of the substrate on the crystal growth and speaks of a “substrate-driven” effect and the consequences on the symmetry planes of the MOF candidates.

#### 4.2.2. Tertiary Hierarchical Composition

Choosing different types of MOFs with secondary hierarchical compositions as building blocks and generating a single large-scale structure lead to a tertiary hierarchical composition. Generating the tertiary structure for simulations is nontrivial, as not only one type but many different types of MOFs interact in

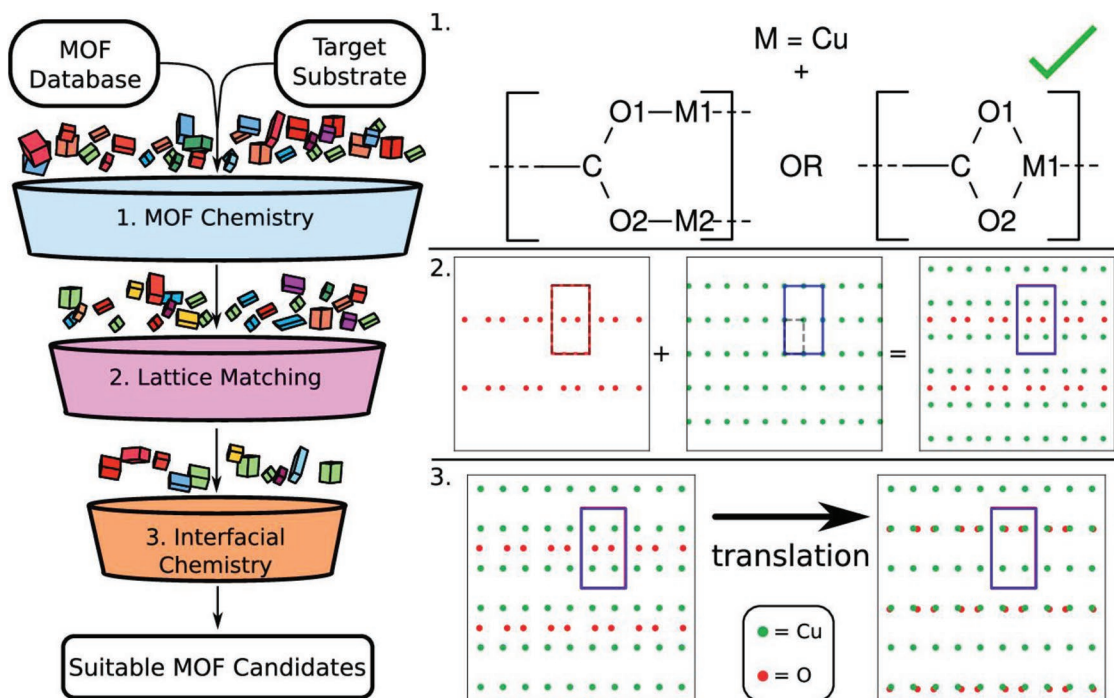


**Figure 19.** Screening steps of the high-throughput algorithm. In the first step only MOFs containing a carboxylate functionality bound to copper pass the test. The second step look for matching supercells, which then can be checked for interfacial bonding in the third and final step. Reproduced with permission.<sup>[178]</sup> Copyright 2018, American Chemical Society.



a single structure. First, the force field needs to be capable of describing every type of MOF, and second, the structure must be generated in a way that can be used for further simulations. For very large systems, it may be advised to use a CG model in which every MOF type is summarized as a single bead. An exemplary system would be an array of pixels where each pixel represents a MOF with a secondary hierarchical composition. Differences in the spatial extension of the building blocks may complicate the structural generation. For example, using a graph-based algorithm with the vertices as building blocks and the edges as the intermolecular bonds would create the structure; however, this approach may not be suitable for building blocks that differ too much from each other, i.e., different building blocks are able to bind with different numbers of other building blocks. In this case, the vertices of the graph must be classified for the structural generation.

Another method would be an MC simulation where the building blocks are randomly placed to find the optimal tertiary hierarchical composition. However, this approach can also become complicated as the calculation of the probabilities needed for the placement increases as the types of different MOFs increases. However, considering the challenges, creating a tertiary hierarchical MOF composition containing secondary and primary hierarchical compositions is more complex than the modeling of hierarchical architecture or hierarchical porosity, but still possible.

## 5. Summary

MOFs offer an intriguing method for the controlled synthesis of functionalized structures across multiple length scales from nm to  $\mu\text{m}$  to the macroscopic scale. The basic molecular building blocks of MOFs provide a large flexibility by permitting many desirable functionally and/or structurally relevant properties for assembly. These building blocks can be stacked hierarchically to create many structures, such as 1D rods, 2D sheets, and 3D architectures. In addition to the architecture, other features of the materials, such as the porosity or chemical composition, can also be organized hierarchically, which is crucial for optimizing specific properties, such as diffusion within a material or directional energy transfer. The resulting hierarchical MOFs vary strongly across several length scales in terms of their framework architecture and pore structure and provide the material science community a powerful toolbox to tailor material properties toward many applications.

Efforts to design MOFs for specific applications can be supplemented by powerful simulation techniques based on MM or DFT. The tremendous growth of both raw computational power and large databases supports both the accuracy and applicability of simulating gas storage and diffusion, drug storage, or high-throughput screening with existing MOF materials for particular applications. However, further refinement of computational tools with respect to both accuracy and transferability toward new systems is needed to allow rational in silico design of hierarchical MOFs toward broad real-world applications. Nevertheless, the prospect of accurate predictions of hypothetical new MOFs and their likely chemical and electronic features is daunting and hard to estimate. A multiscale approach for

simulations could be described as follows: First, take an already investigated primary structure to build a secondary hierarchical structure. If necessary, develop a CG model for the description of the secondary hierarchical structure to reduce computing time. The tertiary hierarchical structure is then obtained by the assembly of the secondary structure to form a macroscopic material. Graph-based algorithms, for instance, could automatically generate very large structures containing all hierarchy types. Currently, (accurate) CG models offer the best trade-off between structural detail and computing effort.

The further advancement of hierarchically structured MOF materials will likely be guided by an interplay of optimized synthesis and processing techniques with enhanced implementation of material modeling. This approach will allow the de novo design and synthesis of high-performing structured materials by specific targeting rationally selected candidates.

## Acknowledgements

Y.L. and M.A. contributed equally to this work. A.S. recognizes support from the Impuls- and Vernetzungsfond of the Helmholtz Association and the Neumann Institute of Computing. M.A., A.S., and M.T. are grateful for funding by the "BioInterfaces in Technology and Medicine Grant" from KIT. Y.L. is thankful for the scholarships from Chinese Scholarship Council. M.T. acknowledges the Helmholtz Association's Initiative and Networking Fund (Grant VH-NG-1147).

## Conflict of Interest

The authors declare no conflict of interest.

## Keywords

hierarchical architecture, metal–organic framework, multiscale modeling

Received: March 19, 2019

Revised: April 9, 2019

Published online:

- [1] E. Ravasz, A.-L. Barabási, *Phys. Rev. E* **2003**, 67, 026112.
- [2] R. Lakes, *Nature* **1993**, 361, 511.
- [3] W. Schwieger, A. G. Machoke, B. Reiprich, T. Weissenberger, T. Selvam, M. Hartmann, in *Zeolites in Catalysis: Properties and Applications*, The Royal Society of Chemistry, London, UK **2017**, p. 103.
- [4] H. S. Stoker, *General, Organic, and Biological Chemistry*, Nelson Education, Hampshire, UK **2012**.
- [5] a) H. Furukawa, K. E. Cordova, M. O'Keeffe, O. M. Yaghi, *Science* **2013**, 341, 1230444; b) S. Kitagawa, R. Kitaura, S. i. Noro, *Angew. Chem., Int. Ed.* **2004**, 43, 2334.
- [6] P. Z. Moghadam, A. Li, S. B. Wiggin, A. Tao, A. G. Maloney, P. A. Wood, S. C. Ward, D. Fairen-Jimenez, *Chem. Mater.* **2017**, 29, 2618.
- [7] a) S. R. Batten, N. R. Champness, X.-M. Chen, J. Garcia-Martinez, S. Kitagawa, L. Öhrström, M. O'Keeffe, M. P. Suh, J. Reedijk, *Pure Appl. Chem.* **2013**, 85, 1715; b) J. Rouquerol, D. Avnir, C. Fairbridge,

- D. Everett, J. Haynes, N. Pernicone, J. Ramsay, K. Sing, K. Unger, *Pure Appl. Chem.* **1994**, 66, 1739.
- [8] H. Deng, C. J. Doonan, H. Furukawa, R. B. Ferreira, J. Towne, C. B. Knobler, B. Wang, O. M. Yaghi, *Science* **2010**, 327, 846.
- [9] S. Furukawa, K. Hirai, Y. Takashima, K. Nakagawa, M. Kondo, T. Tsuruoka, O. Sakata, S. Kitagawa, *Chem. Commun.* **2009**, 34, 5097.
- [10] K. Koh, A. G. Wong-Foy, A. J. Matzger, *Chem. Commun.* **2009**, 41, 6162.
- [11] a) P. Fratzl, R. Weinkamer, *Prog. Mater. Sci.* **2007**, 52, 1263; b) M. A. Meyers, J. McKittrick, P.-Y. Chen, *Science* **2013**, 339, 773.
- [12] H. Xia, J. Zhang, Z. Yang, S. Guo, S. Guo, Q. Xu, *Nano-Micro Lett.* **2017**, 9, 43.
- [13] W. Schwieger, A. G. Machoke, T. Weissenberger, A. Inayat, T. Selvam, M. Klumpp, A. Inayat, *Chem. Soc. Rev.* **2016**, 45, 3353.
- [14] a) J. Heurich, J. Cuevas, W. Wenzel, G. Schön, *Phys. Rev. Lett.* **2002**, 88, 256803; b) A. Schug, M. Weigt, J. N. Onuchic, T. Hwa, H. Szurmant, *Proc. Natl. Acad. Sci. USA* **2009**, 106, 22124; c) K. Lindorff-Larsen, S. Piana, R. O. Dror, D. E. Shaw, *Science* **2011**, 334, 517; d) G. Uguzzoni, S. J. Lovis, F. Oteri, A. Schug, H. Szurmant, M. Weigt, *Proc. Natl. Acad. Sci. USA* **2017**, 114, E2662; e) B. Mattes, Y. Dang, G. Greicius, L. T. Kaufmann, B. Prunusche, J. Rosenbauer, J. Stegmaier, R. Mikut, S. Özbek, G. U. Nienhaus, *ELife* **2018**, 7, e36953.
- [15] a) N. Stock, S. Biswas, *Chem. Rev.* **2011**, 112, 933; b) S. Furukawa, J. Reboul, S. Diring, K. Sumida, S. Kitagawa, *Chem. Soc. Rev.* **2014**, 43, 5700.
- [16] a) V. K. LaMer, R. H. Dinegar, *J. Am. Chem. Soc.* **1950**, 72, 4847; b) S. Wang, C. M. McGuirk, A. d'Aquino, J. A. Mason, C. A. Mirkin, *Adv. Mater.* **2018**, 30, 1800202.
- [17] A. Schug, J. N. Onuchic, *Curr. Opin. Pharmacol.* **2010**, 10, 709.
- [18] S. A. Adcock, J. A. McCammon, *Chem. Rev.* **2006**, 106, 1589.
- [19] a) J. C. Cuevas, J. Heurich, F. Pauly, W. Wenzel, G. Schön, *Nanotechnology* **2003**, 14, R29; b) M. Elbing, R. Ochs, M. Koentopp, M. Fischer, C. von Hänisch, F. Weigend, F. Evers, H. B. Weber, M. Mayor, *Proc. Natl. Acad. Sci. USA* **2005**, 102, 8815.
- [20] a) L. Pastewka, M. O. Robbins, *Proc. Natl. Acad. Sci. USA* **2014**, 111, 3298; b) N. Riley, *J. Fluid Mech.* **2006**, 310, 378.
- [21] P. Hohenberg, W. Kohn, *Phys. Rev.* **1964**, 136, B864.
- [22] a) Technically, a force field allows calculating energies for a given conformation and is hence a potential. The first derivatives of the force fields are forces. b) M. A. González, *JDN* **2011**, 12, 169.
- [23] A. K. Rappe, C. J. Casewit, K. S. Colwell, W. A. Goddard, W. M. Skiff, *J. Am. Chem. Soc.* **1992**, 114, 10024.
- [24] M. A. Addicoat, N. Vankova, I. F. Akter, T. Heine, *J. Chem. Theory Comput.* **2014**, 10, 880.
- [25] S. Bureekaew, S. Amirjalayer, M. Tafipolsky, C. Spickermann, T. K. Roy, R. Schmid, *Phys. Status Solidi B* **2013**, 250, 1128.
- [26] J. K. Bristow, D. Tiana, A. Walsh, *J. Chem. Theory Comput.* **2014**, 10, 4644.
- [27] L. Vanduyfhuys, S. Vandenbrande, T. Verstraelen, R. Schmid, M. Waroquier, V. Van Speybroeck, *J. Comput. Chem.* **2015**, 36, 1015.
- [28] S. L. Mayo, B. D. Olafson, W. A. Goddard, *J. Phys. Chem.* **1990**, 94, 8897.
- [29] A. M. Ferrenberg, R. H. Swendsen, *Comput. Phys.* **1989**, 3, 101.
- [30] S. J. Marrink, H. J. Risselada, S. Yefimov, D. P. Tieleman, A. H. De Vries, *J. Phys. Chem. B* **2007**, 111, 7812.
- [31] F. Paul, C. Wehmeyer, E. T. Abualrous, H. Wu, M. D. Crabtree, J. Schöneberg, J. Clarke, C. Freund, T. R. Weikl, F. Noé, *Nat. Commun.* **2017**, 8, 1095.
- [32] Z. Fang, J. P. Dürholt, M. Kauer, W. Zhang, C. Lochenie, B. Jee, B. Albada, N. Metzler-Nolte, A. Pöppel, B. Weber, M. Muhler, Y. Wang, R. Schmid, R. A. Fischer, *J. Am. Chem. Soc.* **2014**, 136, 9627.
- [33] F.-X. Coudert, A. H. Fuchs, *Coord. Chem. Rev.* **2016**, 307, 211.
- [34] J. A. Greathouse, M. D. Allendorf, *J. Am. Chem. Soc.* **2006**, 128, 10678.
- [35] A. Samanta, T. Furuta, J. Li, *J. Chem. Phys.* **2006**, 125, 084714.
- [36] M. Mattesini, J. M. Soler, F. Ynduráin, *Phys. Rev. B* **2006**, 73, 094111.
- [37] a) G. Garberoglio, A. I. Skoulidas, J. K. Johnson, *J. Phys. Chem. B* **2005**, 109, 13094; b) Q. Yang, C. Zhong, *J. Phys. Chem. B* **2005**, 109, 11862.
- [38] H. Wang, Q.-L. Zhu, R. Zou, Q. Xu, *Chem* **2017**, 2, 52.
- [39] S. S. Han, W.-Q. Deng, W. A. Goddard III, *Angew. Chem., Int. Ed.* **2007**, 46, 6289.
- [40] Y. Chen, Z. Hu, K. M. Gupta, J. Jiang, *J. Phys. Chem. C* **2011**, 115, 21736.
- [41] S. Qiu, M. Xue, G. Zhu, *Chem. Soc. Rev.* **2014**, 43, 6116.
- [42] Q. Yang, C. Zhong, *J. Phys. Chem. B* **2006**, 110, 17776.
- [43] H. Q. Pham, T. Mai, N.-N. Pham-Tran, Y. Kawazoe, H. Mizuseki, D. Nguyen-Manh, *J. Phys. Chem. C* **2014**, 118, 4567.
- [44] B. L. Huang, A. J. H. McGaughey, M. Kaviany, *Int. J. Heat Mass Transfer* **2007**, 50, 393.
- [45] B. Seoane, S. Castellanos, A. Dikhtiarenko, F. Kapteijn, J. Gascon, *Coord. Chem. Rev.* **2016**, 307, 147.
- [46] K. Sumida, K. Liang, J. Reboul, I. A. Ibarra, S. Furukawa, P. Falcaro, *Chem. Mater.* **2017**, 29, 2626.
- [47] B. Tu, Q. Pang, D. Wu, Y. Song, L. Weng, Q. Li, *J. Am. Chem. Soc.* **2014**, 136, 14465.
- [48] A. Umemura, S. Diring, S. Furukawa, H. Uehara, T. Tsuruoka, S. Kitagawa, *J. Am. Chem. Soc.* **2011**, 133, 15506.
- [49] C. Avci, J. Ariñez-Soriano, A. Carné-Sánchez, V. Guillermin, C. Carbonell, I. Imaz, D. Maspoch, *Angew. Chem., Int. Ed.* **2015**, 54, 14417.
- [50] K. M. L. Taylor, W. J. Rieter, W. Lin, *J. Am. Chem. Soc.* **2008**, 130, 14358.
- [51] H. Li, F. Yue, H. Xie, C. Yang, Y. Zhang, L. Zhang, J. Wang, *CrystEngComm* **2018**, 20, 889.
- [52] S. Motoyama, R. Makiura, O. Sakata, H. Kitagawa, *J. Am. Chem. Soc.* **2011**, 133, 5640.
- [53] Y. Ding, Y.-P. Chen, X. Zhang, L. Chen, Z. Dong, H.-L. Jiang, H. Xu, H.-C. Zhou, *J. Am. Chem. Soc.* **2017**, 139, 9136.
- [54] H. J. Lee, W. Cho, M. Oh, *Chem. Commun.* **2012**, 48, 221.
- [55] a) M.-H. Pham, G.-T. Vuong, A.-T. Vu, T.-O. Do, *Langmuir* **2011**, 27, 15261; b) W. J. Rieter, K. M. Taylor, H. An, W. Lin, W. Lin, *J. Am. Chem. Soc.* **2006**, 128, 9024.
- [56] a) P. Sarawade, H. Tan, D. Anjum, D. Cha, V. Polshettiwar, *ChemSusChem* **2014**, 7, 529; b) N. A. Khan, S. H. Jhung, *Coord. Chem. Rev.* **2015**, 285, 11.
- [57] B. Ghalei, K. Sakurai, Y. Kinoshita, K. Wakimoto, A. P. Isfahani, Q. Song, K. Doitomi, S. Furukawa, H. Hirao, H. Kusuda, *Nat. Energy* **2017**, 2, 17086.
- [58] T. H. Bae, J. S. Lee, W. Qiu, W. J. Koros, C. W. Jones, S. Nair, *Angew. Chem., Int. Ed.* **2010**, 49, 9863.
- [59] a) G. Zahn, H. A. Schulze, J. Lippke, S. König, U. Sazama, M. Fröba, P. Behrens, *Microporous Mesoporous Mater.* **2015**, 203, 186; b) A. Schaate, P. Roy, A. Godt, J. Lippke, F. Waltz, M. Wiebcke, P. Behrens, *Chem. - Eur. J.* **2011**, 17, 6643.
- [60] G. Wißmann, A. Schaate, S. Lilienthal, I. Bremer, A. M. Schneider, P. Behrens, *Microporous Mesoporous Mater.* **2012**, 152, 64.
- [61] M.-H. Pham, G.-T. Vuong, F. d. r.-G. Fontaine, T.-O. Do, *Cryst. Growth Des.* **2012**, 12, 3091.
- [62] T. Tsuruoka, S. Furukawa, Y. Takashima, K. Yoshida, S. Isoda, S. Kitagawa, *Angew. Chem., Int. Ed.* **2009**, 48, 4739.
- [63] A. Kojtari, P. J. Carroll, H.-F. Ji, *CrystEngComm* **2014**, 16, 2885.
- [64] L. Zou, C.-C. Hou, Z. Liu, H. Pang, Q. Xu, *J. Am. Chem. Soc.* **2018**, 140, 15393.

- [65] M. Gao, L. Zeng, J. Nie, G. Ma, *RSC Adv.* **2016**, *6*, 7078.
- [66] a) M. S. Yao, W. X. Tang, G. E. Wang, B. Nath, G. Xu, *Adv. Mater.* **2016**, *28*, 5229; b) W.-w. Zhan, Q. Kuang, J.-z. Zhou, X.-j. Kong, Z.-x. Xie, L.-s. Zheng, *J. Am. Chem. Soc.* **2013**, *135*, 1926.
- [67] W. Zhang, Z.-Y. Wu, H.-L. Jiang, S.-H. Yu, *J. Am. Chem. Soc.* **2014**, *136*, 14385.
- [68] H. Yu, X. Qiu, P. Neelakanda, L. Deng, N. M. Khashab, S. P. Nunes, K.-V. Peinemann, *Sci. Rep.* **2015**, *5*, 15275.
- [69] A. Kondo, C. C. Tiew, F. Moriguchi, K. Maeda, *Dalton Trans.* **2013**, *42*, 15267.
- [70] L. Cao, T. Wang, C. Wang, *Chin. J. Chem.* **2018**, *36*, 754.
- [71] L. Cao, Z. Lin, W. Shi, Z. Wang, C. Zhang, X. Hu, C. Wang, W. Lin, *J. Am. Chem. Soc.* **2017**, *139*, 7020.
- [72] M. Hu, S. Ishihara, Y. Yamauchi, *Angew. Chem., Int. Ed.* **2013**, *52*, 1235.
- [73] S. Zhao, Y. Wang, J. Dong, C.-T. He, H. Yin, P. An, K. Zhao, X. Zhang, C. Gao, L. Zhang, *Nat. Energy* **2016**, *1*, 16184.
- [74] a) X. Sun, K.-H. Wu, R. Sakamoto, T. Kusamoto, H. Maeda, H. Nishihara, *Chem. Lett.* **2017**, *46*, 1072; b) T. Pal, T. Kambe, T. Kusamoto, M. L. Foo, R. Matsuoka, R. Sakamoto, H. Nishihara, *ChemPlusChem* **2015**, *80*, 1255; c) N. Lahiri, N. Lotfizadeh, R. Tsuchikawa, V. V. Deshpande, J. Louie, *J. Am. Chem. Soc.* **2016**, *139*, 19; d) X. Huang, P. Sheng, Z. Tu, F. Zhang, J. Wang, H. Geng, Y. Zou, C.-a. Di, Y. Yi, Y. Sun, W. Xu, D. Zhu, *Nat. Commun.* **2015**, *6*, 7408; e) A. J. Clough, J. M. Skelton, C. A. Downes, A. A. De La Rosa, J. W. Yoo, A. Walsh, B. C. Melot, S. C. Marinescu, *J. Am. Chem. Soc.* **2017**, *139*, 10863.
- [75] a) V. c. Rubio-Giménez, S. Tatay, F. Volatron, F. J. Martínez-Casado, C. Martí-Gastaldo, E. Coronado, *J. Am. Chem. Soc.* **2016**, *138*, 2576; b) R. Makiura, S. Motoyama, Y. Umemura, H. Yamanaka, O. Sakata, H. Kitagawa, *Nat. Mater.* **2010**, *9*, 565; c) R. Dong, M. Pfeiffermann, H. Liang, Z. Zheng, X. Zhu, J. Zhang, X. Feng, *Angew. Chem., Int. Ed.* **2015**, *54*, 12058; d) R. Dong, Z. Zheng, D. C. Tranca, J. Zhang, N. Chandrasekhar, S. Liu, X. Zhuang, G. Seifert, X. Feng, *Chem. - Eur. J.* **2017**, *23*, 2255; e) R. Makiura, R. Usui, Y. Sakai, A. Nomoto, A. Ogawa, O. Sakata, A. Fujiwara, *ChemPlusChem* **2014**, *79*, 1352; f) R. Makiura, O. Konovalov, *Sci. Rep.* **2013**, *3*, 2506; g) M. Tsotsalas, A. Umemura, F. Kim, Y. Sakata, J. Reboul, S. Kitagawa, S. Furukawa, *J. Mater. Chem.* **2012**, *22*, 10159.
- [76] T. Rodenas, I. Luz, G. Prieto, B. Seoane, H. Miro, A. Corma, F. Kapteijn, F. X. L. i Xamena, J. Gascon, *Nat. Mater.* **2015**, *14*, 48.
- [77] a) G. E. Gomez, M. C. Bernini, E. V. Brusau, G. E. Narda, D. Vega, A. M. Kaczmarek, R. Van Deun, M. Nazzarro, *Dalton Trans.* **2015**, *44*, 3417; b) P.-Z. Li, Y. Maeda, Q. Xu, *Chem. Commun.* **2011**, *47*, 8436; c) P. Armo-Ochoa, L. Welte, R. González-Prieto, P. J. Sanz Miguel, C. J. Gómez-García, E. Mateo-Martí, S. Delgado, J. Gómez-Herrero, F. Zamora, *Chem. Commun.* **2010**, *46*, 3262; d) P. Chandrasekhar, A. Mukhopadhyay, G. Savitha, J. N. Moorthy, *J. Mater. Chem. A* **2017**, *5*, 5402.
- [78] X. Wang, C. Chi, K. Zhang, Y. Qian, K. M. Gupta, Z. Kang, J. Jiang, D. Zhao, *Nat. Commun.* **2017**, *8*, 14460.
- [79] A. Abhervé, S. Mañas-Valero, M. Clemente-León, E. Coronado, *Chem. Sci.* **2015**, *6*, 4665.
- [80] a) T. Araki, A. Kondo, K. Maeda, *Chem. Commun.* **2013**, *49*, 552; b) Y. Peng, Y. Li, Y. Ban, W. Yang, *Angew. Chem., Int. Ed.* **2017**, *56*, 9757; c) A. Gallego, C. Hermosa, O. Castillo, I. Berlanga, C. J. Gómez-García, E. Mateo-Martí, J. I. Martínez, F. Flores, C. Gómez-Navarro, J. Gómez-Herrero, S. Delgado, F. Zamora, *Adv. Mater.* **2013**, *25*, 2141.
- [81] M. J. Cliffe, E. Castillo-Martínez, Y. Wu, J. Lee, A. C. Forse, F. C. N. Firth, P. Z. Moghadam, D. Fairen-Jimenez, M. W. Gaultois, J. A. Hill, O. V. Magdysyuk, B. Slater, A. L. Goodwin, C. P. Grey, *J. Am. Chem. Soc.* **2017**, *139*, 5397.
- [82] a) P. Falcaro, D. Buso, A. J. Hill, C. M. Doherty, *Adv. Mater.* **2012**, *24*, 3153; b) I. Stassen, N. Burtch, A. Talin, P. Falcaro, M. Allendorf, R. Ameloot, *Chem. Soc. Rev.* **2017**, *46*, 3185.
- [83] a) J. Liu, B. Lukose, O. Shekhah, H. K. Arslan, P. Weidler, H. Gliemann, S. Bräse, S. Grosjean, A. Godt, X. Feng, K. Müllen, I.-B. Magdau, T. Heine, C. Wöll, *Sci. Rep.* **2012**, *2*, 921; b) S. Sakaida, K. Otsubo, O. Sakata, C. Song, A. Fujiwara, M. Takata, H. Kitagawa, *Nat. Chem.* **2016**, *8*, 377.
- [84] Y. Zhao, N. Kornienko, Z. Liu, C. Zhu, S. Asahina, T.-R. Kuo, W. Bao, C. Xie, A. Hexemer, O. Terasaki, P. Yang, O. M. Yaghi, *J. Am. Chem. Soc.* **2015**, *137*, 2199;
- [85] a) N. Campagnol, T. Van Assche, T. Boudewijns, J. Denayer, K. Binnemans, D. De Vos, J. Fransaer, *J. Mater. Chem. A* **2013**, *1*, 5827; b) W.-J. Li, J. Lü, S.-Y. Gao, Q.-H. Li, R. Cao, *J. Mater. Chem. A* **2014**, *2*, 19473; c) W.-J. Li, J. Liu, Z.-H. Sun, T.-F. Liu, J. Lü, S.-Y. Gao, C. He, R. Cao, J.-H. Luo, *Nat. Commun.* **2016**, *7*, 11830.
- [86] a) Y. Chen, S. Li, X. Pei, J. Zhou, X. Feng, S. Zhang, Y. Cheng, H. Li, R. Han, B. Wang, *Angew. Chem., Int. Ed.* **2016**, *55*, 3419; b) V. M. Aceituno Melgar, H. T. Kwon, J. Kim, *J. Membr. Sci.* **2014**, *459*, 190; c) L. Fan, M. Xue, Z. Kang, H. Li, S. Qiu, *J. Mater. Chem.* **2012**, *22*, 25272.
- [87] a) E. Ahvenniemi, M. Karppinen, *Chem. Commun.* **2016**, *52*, 1139; b) K. B. Lausund, O. Nilsen, *Nat. Commun.* **2016**, *7*, 13578.
- [88] a) H. Walch, J. Dienstmaier, G. Eder, R. Gutzler, S. Schlögl, T. Sirtl, K. Das, M. Schmittel, M. Lackinger, *J. Am. Chem. Soc.* **2011**, *133*, 7909; b) Y. Li, J. Xiao, T. E. Shubina, M. Chen, Z. Shi, M. Schmid, H.-P. Steinrück, J. M. Gottfried, N. Lin, *J. Am. Chem. Soc.* **2012**, *134*, 6401; c) B. Wurster, D. Grumelli, D. Hötger, R. Gutzler, K. Kern, *J. Am. Chem. Soc.* **2016**, *138*, 3623.
- [89] I. Stassen, M. Styles, G. Greci, H. Van Gorp, W. Vanderlinden, S. De Feyter, P. Falcaro, D. De Vos, P. Vereecken, R. Ameloot, *Nat. Mater.* **2016**, *15*, 304.
- [90] P. Falcaro, R. Ricco, C. M. Doherty, K. Liang, A. J. Hill, M. J. Styles, *Chem. Soc. Rev.* **2014**, *43*, 5513.
- [91] a) M. Hou, H. Zhao, Y. Feng, J. Ge, *Bioresources Bioprocessing* **2017**, *4*, 40; b) J.-L. Zhuang, D. Ar, X.-J. Yu, J.-X. Liu, A. Terfort, *Adv. Mater.* **2013**, *25*, 4631.
- [92] C. Carbonell, I. Imaz, D. Maspoch, *J. Am. Chem. Soc.* **2011**, *133*, 2144.
- [93] J. J. Gassensmith, P. M. Erne, W. F. Paxton, C. Valente, J. F. Stoddart, *Langmuir* **2011**, *27*, 1341.
- [94] J.-L. Zhuang, D. Ceglarek, S. Pethuraj, A. Terfort, *Adv. Funct. Mater.* **2011**, *21*, 1442.
- [95] a) A. Schaller, A. Ullrich, S. Horn, D. Volkmer, *Chem. Commun.* **2015**, *51*, 12494; b) B. K. Keitz, C. J. Yu, J. R. Long, R. Ameloot, *Angew. Chem., Int. Ed.* **2014**, *53*, 5561.
- [96] J. Zhuang, J. Friedel, A. Terfort, *Beilstein J. Nanotechnol.* **2012**, *3*, 570.
- [97] K. Hirai, K. Sada, *Chem. Commun.* **2017**, *53*, 5275.
- [98] G. Lu, O. K. Farha, W. Zhang, F. Huo, J. T. Hupp, *Adv. Mater.* **2012**, *24*, 3970.
- [99] a) H. Kim, M. S. Lah, *Dalton Trans.* **2017**, *46*, 6146; b) V. Valtchev, *Chem. Mater.* **2002**, *14*, 4371.
- [100] C.-H. Kuo, Y. Tang, L.-Y. Chou, B. T. Sneed, C. N. Brodsky, Z. Zhao, C.-K. Tsung, *J. Am. Chem. Soc.* **2012**, *134*, 14345.
- [101] S. Aguado, J. Canivet, D. Farrusseng, *Chem. Commun.* **2010**, *46*, 7999.
- [102] S. Sorribas, B. Zornoza, C. Téllez, J. Coronas, *Chem. Commun.* **2012**, *48*, 9388.
- [103] Y. Liu, W. Zhang, S. Li, C. Cui, J. Wu, H. Chen, F. Huo, *Chem. Mater.* **2014**, *26*, 1119.
- [104] a) W. Zhi, W. Li, J. Cha, G. Zheng, Y. Yuan, M. McDowell, P. Hsu, C. Yi, *Nat. Commun.* **2013**, *4*, 1331; b) G. Zhang, S. Hou, H. Zhang, W. Zeng, F. Yan, C. C. Li, H. Duan, *Adv. Mater.* **2015**, *27*, 2400; c) Y. Zhao, X. Li, J. Liu, C. Wang, Y. Zhao, G. Yue, *ACS Appl. Mater. Interfaces* **2016**, *8*, 6472.

- [105] a) G. Liang, J. Xu, X. Wang, *J. Am. Chem. Soc.* **2009**, *131*, 5378; b) X. Cao, L. Dai, L. Wang, J. Liu, J. Lei, *Mater. Lett.* **2015**, *161*, 682.
- [106] W. Li, Y. Zhang, Z. Xu, Q. Meng, Z. Fan, S. Ye, G. Zhang, *Angew. Chem., Int. Ed.* **2016**, *55*, 955.
- [107] a) Y. Yang, F. Wang, Q. Yang, Y. Hu, H. Yan, Y.-Z. Chen, H. Liu, G. Zhang, J. Lu, H.-L. Jiang, H. Xu, *ACS Appl. Mater. Interfaces* **2014**, *6*, 18163; b) G.-Y. Jeong, R. Ricco, K. Liang, J. Ludwig, J.-O. Kim, P. Falcaro, D.-P. Kim, *Chem. Mater.* **2015**, *27*, 7903.
- [108] A. Carné-Sánchez, I. Imaz, M. Cano-Sarabia, D. MasPOCH, *Nat. Chem.* **2013**, *5*, 203.
- [109] a) J. Huo, J. Aguilera-Sigalat, S. El-Hankari, D. Bradshaw, *Chem. Sci.* **2015**, *6*, 1938; b) R. Ameloot, F. Vermoortele, W. Vanhove, M. B. J. Roeffaers, B. F. Sels, D. E. De Vos, *Nat. Chem.* **2011**, *3*, 382.
- [110] L. Peng, J. Zhang, J. Li, B. Han, Z. Xue, B. Zhang, J. Shi, G. Yang, *J. Colloid Interface Sci.* **2014**, *416*, 198.
- [111] W. Zhang, X. Jiang, Y. Zhao, A. Carné-Sánchez, V. Malgras, J. Kim, J. H. Kim, S. Wang, J. Liu, J.-S. Jiang, Y. Yamauchi, M. Hu, *Chem. Sci.* **2017**, *8*, 3538.
- [112] W. Liu, J. Huang, Q. Yang, S. Wang, X. Sun, W. Zhang, J. Liu, F. Huo, *Angew. Chem., Int. Ed.* **2017**, *56*, 5512.
- [113] Z. Wang, J. Wang, M. Li, K. Sun, C.-j. Liu, *Sci. Rep.* **2014**, *4*, 5939.
- [114] Y. Chen, F. Chen, S. Zhang, Y. Cai, S. Cao, S. Li, W. Zhao, S. Yuan, X. Feng, A. Cao, X. Ma, B. Wang, *J. Am. Chem. Soc.* **2017**, *139*, 16482.
- [115] O. Halevi, J. M. R. Tan, P. S. Lee, S. Magdassi, *Adv. Sustainable Syst.* **2018**, *2*, 1700150.
- [116] S. Choi, T. Kim, H. Ji, H. J. Lee, M. Oh, *J. Am. Chem. Soc.* **2016**, *138*, 14434.
- [117] N. Yanai, M. Sindoro, J. Yan, S. Granick, *J. Am. Chem. Soc.* **2013**, *135*, 34.
- [118] M. Pang, A. J. Cairns, Y. Liu, Y. Belmabkhout, H. C. Zeng, M. Eddaoudi, *J. Am. Chem. Soc.* **2013**, *135*, 10234.
- [119] C. Avci, I. Imaz, A. Carné-Sánchez, J. A. Pariente, N. Tasio, J. Pérez-Carvajal, M. I. Alonso, A. Blanco, M. Dijkstra, C. López, D. MasPOCH, *Nat. Chem.* **2017**, *10*, 78.
- [120] Y. Yan, P. Gu, S. Zheng, M. Zheng, H. Pang, H. Xue, *J. Mater. Chem. A* **2016**, *4*, 19078.
- [121] Y. C. Tan, H. C. Zeng, *Adv. Funct. Mater.* **2017**, *27*, 1703765.
- [122] P. Falcaro, K. Okada, T. Hara, K. Ikigaki, Y. Tokudome, A. W. Thornton, A. J. Hill, T. Williams, C. Doonan, M. Takahashi, *Nat. Mater.* **2017**, *16*, 342.
- [123] L. Lupica-Spagnolo, D. J. Ward, J.-J. Marie, S. Lympieropoulou, D. Bradshaw, *Chem. Commun.* **2018**, *54*, 8506.
- [124] C. Avci, J. Ariñez-Soriano, A. Carné-Sánchez, V. Guillermin, C. Carbonell, I. Imaz, D. MasPOCH, *Angew. Chem., Int. Ed.* **2015**, *54*, 14417.
- [125] M. W. Anderson, J. T. Gebbie-Rayet, A. R. Hill, N. Farida, M. P. Atfield, P. Cubillas, V. A. Blatov, D. M. Proserpio, D. Akporiaye, B. Arstad, J. D. Gale, *Nature* **2017**, *544*, 456.
- [126] J. Caro, *Chem. Soc. Rev.* **2016**, *45*, 3468.
- [127] X.-Y. Yang, L.-H. Chen, Y. Li, J. C. Rooke, C. Sanchez, B.-L. Su, *Chem. Soc. Rev.* **2017**, *46*, 481.
- [128] a) X.-X. Huang, L.-G. Qiu, W. Zhang, Y.-P. Yuan, X. Jiang, A.-J. Xie, Y.-H. Shen, J.-F. Zhu, *CrystEngComm* **2012**, *14*, 1613; b) L. G. Qiu, T. Xu, Z. Q. Li, W. Wang, Y. Wu, X. Jiang, X. Y. Tian, L. D. Zhang, *Angew. Chem., Int. Ed.* **2008**, *47*, 9487.
- [129] L. H. Wee, C. Wiktor, S. Turner, W. Vanderlinden, N. Janssens, S. R. Bajpe, K. Houthoofd, G. Van Tendeloo, S. De Feyter, C. E. Kirschhock, *J. Am. Chem. Soc.* **2012**, *134*, 10911.
- [130] S. Diring, S. Furukawa, Y. Takashima, T. Tsuruoka, S. Kitagawa, *Chem. Mater.* **2010**, *22*, 4531.
- [131] C. Duan, F. Li, H. Zhang, J. Li, X. Wang, H. Xi, *RSC Adv.* **2017**, *7*, 52245.
- [132] S. Cao, G. Gody, W. Zhao, S. Perrier, X. Peng, C. Ducati, D. Zhao, A. K. Cheetham, *Chem. Sci.* **2013**, *4*, 3573.
- [133] L.-B. Sun, J.-R. Li, J. Park, H.-C. Zhou, *J. Am. Chem. Soc.* **2011**, *134*, 126.
- [134] S. Alizadeh, D. Nematollahi, *J. Am. Chem. Soc.* **2017**, *139*, 4753.
- [135] K. Shen, L. Zhang, X. Chen, L. Liu, D. Zhang, Y. Han, J. Chen, J. Long, R. Luque, Y. Li, *Science* **2018**, *359*, 206.
- [136] Y. Zhao, J. Zhang, B. Han, J. Song, J. Li, Q. Wang, *Angew. Chem., Int. Ed.* **2011**, *50*, 636.
- [137] L. Peng, J. Zhang, Z. Xue, B. Han, X. Sang, C. Liu, G. Yang, *Nat. Commun.* **2014**, *5*, 4465.
- [138] J. Reboul, S. Furukawa, N. Horike, M. Tsotsalas, K. Hirai, H. Uehara, M. Kondo, N. Louvain, O. Sakata, S. Kitagawa, *Nat. Mater.* **2012**, *11*, 717.
- [139] Y. Kim, T. Yang, G. Yun, M. B. Ghasemian, J. Koo, E. Lee, S. J. Cho, K. Kim, *Angew. Chem., Int. Ed.* **2015**, *54*, 13273.
- [140] P. Yang, F. Mao, Y. Li, Q. Zhuang, J. Gu, *Chem. - Eur. J.* **2018**, *24*, 2962.
- [141] X. Yang, S. Wu, P. Wang, L. Yang, *J. Solid State Chem.* **2018**, *258*, 220.
- [142] W. Zhang, Y. Liu, G. Lu, Y. Wang, S. Li, C. Cui, J. Wu, Z. Xu, D. Tian, W. Huang, J. S. DuCheneu, W. D. Wei, H. Chen, Y. Yang, F. Huo, *Adv. Mater.* **2015**, *27*, 2923.
- [143] F. Meng, S. Zhang, L. Ma, W. Zhang, M. Li, T. Wu, H. Li, T. Zhang, X. Lu, F. Huo, J. Lu, *Adv. Mater.* **2018**, *30*, 1803263.
- [144] S. Yuan, L. Zou, J.-S. Qin, J. Li, L. Huang, L. Feng, X. Wang, M. Bosch, A. Alsalmé, T. Cagin, *Nat. Commun.* **2017**, *8*, 15356.
- [145] R. B. Getman, Y.-S. Bae, C. E. Wilmer, R. Q. Snurr, *Chem. Rev.* **2012**, *112*, 703.
- [146] J. P. Dürholt, J. Keupp, R. Schmid, *Eur. J. Inorg. Chem.* **2016**, *2016*, 4517.
- [147] M. Alhamami, H. Doan, C.-H. Cheng, *Materials* **2014**, *7*, 3198.
- [148] a) J. C. Noveron, M. S. Lah, R. E. Del Sesto, A. M. Arif, J. S. Miller, P. J. Stang, *J. Am. Chem. Soc.* **2002**, *124*, 6613; b) J. C. MacDonald, P. C. Dorrestein, M. M. Pilley, M. M. Foote, J. L. Lundburg, R. W. Henning, A. J. Schultz, J. L. Manson, *J. Am. Chem. Soc.* **2000**, *122*, 11692.
- [149] a) J. Ren, N. M. Musyoka, H. W. Langmi, B. C. North, M. Mathe, X. Kang, *Int. J. Hydrogen Energy* **2014**, *39*, 14912; b) J. Ren, H. W. Langmi, N. M. Musyoka, M. Mathe, X. Kang, S. Liao, *Mater. Today: Proc.* **2015**, *2*, 3964.
- [150] K. A. McDonald, J. I. Feldblyum, K. Koh, A. G. Wong-Foy, A. J. Matzger, *Chem. Commun.* **2015**, *51*, 11994.
- [151] H. J. Lee, Y. J. Cho, W. Cho, M. Oh, *ACS Nano* **2012**, *7*, 491.
- [152] T. Li, J. E. Sullivan, N. L. Rosi, *J. Am. Chem. Soc.* **2013**, *135*, 9984.
- [153] T. Ishiwata, A. Michibata, K. Kokado, S. Ferlay, M. W. Hosseini, K. Sada, *Chem. Commun.* **2018**, *54*, 1437.
- [154] C. Li, S. Dong, R. Tang, X. Ge, Z. Zhang, C. Wang, Y. Lu, L. Yin, *Energy Environ. Sci.* **2018**, *11*, 3201.
- [155] K. Hirai, S. Furukawa, M. Kondo, M. Meilikhov, Y. Sakata, O. Sakata, S. Kitagawa, *Chem. Commun.* **2012**, *48*, 6472.
- [156] J. Zhuang, L. Y. Chou, B. T. Sneed, Y. Cao, P. Hu, L. Feng, C. K. Tsung, *Small* **2015**, *11*, 5551.
- [157] Y. Yoo, H.-K. Jeong, *Cryst. Growth Des.* **2010**, *10*, 1283.
- [158] a) J. Tang, R. R. Salunkhe, J. Liu, N. L. Torad, M. Imura, S. Furukawa, Y. Yamauchi, *J. Am. Chem. Soc.* **2015**, *137*, 1572; b) J. Xu, S. Liu, Y. Liu, *RSC Adv.* **2016**, *6*, 52137.
- [159] P. Á. Szilágyi, M. Lutz, J. Gascon, J. Juan-Alcaniz, J. van Esch, F. Kapteijn, H. Geerlings, B. Dam, R. van de Krol, *CrystEngComm* **2013**, *15*, 6003.
- [160] a) V. Chernikova, O. Shekhah, M. Eddaoudi, *ACS Appl. Mater. Interfaces* **2016**, *8*, 20459; b) J.-L. Zhuang, A. Terfort, C. Wöll, *Coord. Chem. Rev.* **2016**, *307*, 391.
- [161] B. Liu, M. Ma, D. Zacher, A. Bétard, K. Yuseenko, N. Metzler-Nolte, C. Wöll, R. A. Fischer, *J. Am. Chem. Soc.* **2011**, *133*, 1734.

- [162] a) D. Zacher, K. Yusenko, A. Bétard, S. Henke, M. Molon, T. Ladnorg, O. Shekhah, B. Schüpbach, T. de los Arcos, M. Krasnopolski, *Chem. - Eur. J.* **2011**, *17*, 1448; b) O. Shekhah, K. Hirai, H. Wang, H. Uehara, M. Kondo, S. Diring, D. Zacher, R. A. Fischer, O. Sakata, S. Kitagawa, *Dalton Trans.* **2011**, *40*, 4954.
- [163] M. Meilikhov, S. Furukawa, K. Hirai, R. A. Fischer, S. Kitagawa, *Angew. Chem., Int. Ed.* **2013**, *52*, 341.
- [164] M. Tu, R. A. Fischer, *J. Mater. Chem. A* **2014**, *2*, 2018.
- [165] Z. Wang, J. Liu, B. Lukose, Z. Gu, P. G. Weidler, H. Gliemann, T. Heine, C. Wöll, *Nano Lett.* **2014**, *14*, 1526.
- [166] M. Tu, S. Wannapaiboon, R. A. Fischer, *Dalton Trans.* **2013**, *42*, 16029.
- [167] L. Heinke, M. Cakici, M. Dommaschk, S. Grosjean, R. Herges, S. Bräse, C. Wöll, *ACS Nano* **2014**, *8*, 1463.
- [168] V. Chernikova, O. Shekhah, I. Spanopoulos, P. N. Trikalitis, M. Eddaoudi, *Chem. Commun.* **2017**, *53*, 6191.
- [169] S. Schmitt, M. Silvestre, M. Tsotsalas, A.-L. Winkler, A. Shahnas, S. Grosjean, F. Laye, H. Gliemann, J. Lahann, S. Bräse, *ACS Nano* **2015**, *9*, 4219.
- [170] Z. Song, F. Qiu, E. W. Zaia, Z. Wang, M. Kunz, J. Guo, M. Brady, B. Mi, J. J. Urban, *Nano Lett.* **2017**, *17*, 6752.
- [171] I. Stassen, I. Boldog, C. Steuwe, D. De Vos, M. Roeffaers, S. Furukawa, R. Ameloot, *Chem. Commun.* **2017**, *53*, 7222.
- [172] J. A. Boissonnault, A. G. Wong-Foy, A. J. Matzger, *J. Am. Chem. Soc.* **2017**, *139*, 14841.
- [173] X. Xu, Y. Sun, Q. Zhang, S. Wang, L. Zhang, Z. Wu, G. Lu, *ChemistrySelect* **2016**, *1*, 1763.
- [174] Y. Gu, Y. n. Wu, L. Li, W. Chen, F. Li, S. Kitagawa, *Angew. Chem., Int. Ed.* **2017**, *56*, 15658.
- [175] M. A. Addicoat, D. E. Coupry, T. Heine, *J. Phys. Chem. A* **2014**, *118*, 9607.
- [176] S. Amirjalayer, M. Tafipolsky, R. Schmid, *J. Phys. Chem. Lett.* **2014**, *5*, 3206.
- [177] R. Semino, J. P. Dürholt, R. Schmid, G. Maurin, *J. Phys. Chem. C* **2017**, *121*, 21491.
- [178] A. Tarzia, M. Takahashi, P. Falcaro, A. W. Thornton, C. J. Doonan, D. M. Huang, *ACS Appl. Mater. Interfaces* **2018**, *10*, 40938.